UNIVERSITÀ
DEGLI STUDI
DI PADOVA

Head Office: Università degli Studi di Padova

Department of Molecular Medicine

Ph.D. COURSE IN: Molecular Medicine

CURRICULUM: Biomedicine

XXXII SERIES

ROLE OF YAP/TAZ IN LIVER TUMORIGENESIS AND MAMMARY GLAND CELLS DEDIFFERENTIATION

Thesis written with the financial contribution of Fondazione Cariparo

Supervisor: Prof. Stefano Piccolo

Ph.D. student : Romy Lucon Xiccato

INDEX

PUBLICATIONS

Chang, L., Azzolin L., Di Biagio D., Zanconato F., Battilana G., **Lucon Xiccato R**., Aragona M., Giulitti S., Panciera T., Gandin A., Sigismondo G., Krijgsveld J., Fassan M., Brusatin G., Cordenonsi M., Piccolo S. (2018) 'The SWI/SNF complex is a mechanoregulated inhibitor of YAP and TAZ', *Nature* (2018). doi:10.1038/s41586-018-0658-1

The work presented in the first part of thesis was ideated and coordinated by Dr. Lei Chang, Prof. Michelangelo Cordenonsi and Prof. Stefano Piccolo.
I performed experiments under their supervision, together with Dr. Luca Azzolin and Dr. Daniele Di Biagio.

The work presented in the second part of this thesis was ideated and coordinated by Dr. Tito Panciera, Prof. Michelangelo Cordenonsi and Prof. Stefano Piccolo.
I performed experiments under their supervision, together with Dr. Luca Azzolin and Dr. Daniele Di Biagio.

ABSTRACT

YAP and TAZ are two transcriptional co-factors implicated in regulating fundamental biological processes, such as proliferation, regeneration, cell fate plasticity and tumorigenesis. Many upstream stimuli, such as the Hippo pathway and biomechanical inputs, regulate YAP/TAZ function. However, to date, our understanding of YAP/TAZ regulation is limited.

Here I present our work on the role of SWI/SNF chromatin-remodeling complex, as YAP/TAZ nuclear inhibitor. By different *in vitro* assays, we found that SWI/SNF inactivation remarkably promotes YAP/TAZ-driven cell proliferation, and that the SWI/SNF component more relevant for this control is the tumor suppressor Arid1a, acting as YAP/TAZ inhibitor. In the first part of this thesis, we validate SWI/SNF tumor suppressive functions *in vivo*, focusing on liver tumorigenesis induced either by Hippo pathway inactivation or by chronic damage induced by the hepato-toxic compound DDC. In both of these set ups, we found that inactivation of Arid1a robustly activates YAP/TAZ, giving rise to liver tumorigenesis. Our findings prompted us to speculate that SWI/SNF can exert its tumor-suppressor function by inhibiting YAP/TAZ.

Work recently published from our laboratory showed that ectopic expression of YAP/TAZ may confer stemness characteristics to normal mammary luminal differentiated cells (LD), converting them into Mammary Stem Cells-like cells (yMaSCs). In the second part of this thesis we expanded on this topic, and characterized early colonies arising from LD cells after YAP transfection. We found that a significant fraction of the genes upregulated upon LD to yMaSC transformation corresponds to genes specially expressed in the fetal mammary gland. This suggests that early colonies represent a fetal-like cellular state that is distinct from adult progenitors. In sum, this work focuses on the nuclear regulation of YAP/TAZ, offering shed new light on the

enigmatic functions of an important tumor suppressor (ARID1a), and also expand on the biological consequences of YAP-induced stemness and cell plasticity.

INTRODUCTION

YAP/TAZ and their regulations

YAP (Yes-associated protein) and TAZ (transcriptional co-activator with PDZ-binding motif, also known as WWTR1) are homologous transcriptional co-factors, which were first discovered as the nuclear effectors of the Hippo pathway (Figure 1a). The Hippo pathway is a signalling cascade (conserved from *Drosophila melanogaster* to mammals) responsible for organ size control and tissue regeneration (Harvey et al., 2013; Hansen et al., 2015). The Hippo pathway core is composed by two kinase complexes: MST1/2 and LATS1/2. The sterile serine/threonine 20-like kinases MST1 and MST2 (Hippo in *Drosophila*) bind their adaptor protein Salvador homologue 1 (SAV1, also known as WW45) to form an active complex. They phosphorylate and activate the large tumour suppressor 1 (LATS1) and 2 (LATS2) and their regulatory subunits MOB1 A/B. The activation of the LATS1/2-MOB1A/B complex results in the phosphorylation of multiple serine residues of YAP and TAZ, which in turn leads to their cytoplasmic retention through interaction with 14-3-3 proteins. Furthermore, the phosphorylation of YAP/TAZ by LATS1/2 primes for additional phosphorylations, generating a "phosphodegron" recognized by β-TRCP, an adaptor for the SCF E3 ubiquitin ligase, that addresses YAP/TAZ to proteasomal degradation (Hansen et al., 2015). Inactivation of the Hippo pathway leads to nuclear accumulation of YAP/TAZ and activation of target gene expression.

Beside the Hippo pathway, many other upstream regulators of YAP/TAZ have been so far described.

These include cell shape and polarity, mechanical stimuli from the microenvironment, soluble signals (mediated by the Wnt and GPCR pathways), and cell metabolism (Piccolo et al., 2014). For what concerns cell-cell adhesion and apical-basal polarity, these elements have been reported as regulators of YAP/TAZ localization and phosphorylation through the Hippo cascade. One of the factors involved in this role is

the NF2 (neurofibromatosis type 2, also known as Merlin) tumor suppressor. At cell-cell junctions, Merlin may promote the assembly of the appropriate protein scaffolds that allow LATS activation and YAP phosphorylation (Aragona et al., 2013). Another important aspect is that the normal epithelial architecture, characterized by specialized cell-cell junctions and apicobasal polarity, is a potent suppressor of YAP/TAZ activity (Martin-Belmonte et al., 2012). Mechanistically, this has been linked to different polarity proteins, in particular to the membrane localization of Scribble, a key cell polarity determinant that serves as adaptor for the Hippo kinases by assembling a complex containing MST, LATS, and TAZ, required for MST-mediated activation of LATS (Cordenonsi et al., 2011).

Hippo-independent regulation of YAP/TAZ activity are emerging as fundamental signals regulating YAP/TAZ biology. Mechanical inputs are a case in point: when a single cell is allowed to stretch over the ECM, the cytoskeletal adaptation to the spread cell shape causes YAP/TAZ activation and nuclear accumulation, promoting proliferation and inhibiting differentiation (Dupont et al., 2011). Conversely, when a cell is forced to assume a round and compact shape - for example in a small ECM island -, YAP/TAZ gets excluded from the nucleus. YAP/TAZ can also respond to changes in ECM stiffness: a rigid ECM keeps active YAP/TAZ to the nucleus, while more compliant matrices favour YAP/TAZ inactivation.

Another form of mechanical regulation of YAP/TAZ can be provided by cell density. The key role of YAP/TAZ inactivation in the contact inhibition of proliferation, has been explained with a “two-step model”: when cells start to make contact with each other, YAP/TAZ get phosphorylated by LATS; successively, as cells continue to proliferate, resulting in a crowded monolayer, the reduction in area will impair YAP/TAZ mechanical pathway causing their inhibition (Aragona et al., 2013).

YAP/TAZ are not only messengers of the cell architectures, but also orchestrate the intracellular response to soluble growth factors, as the Wnt family growth factors. In

the absence of Wnt, cytoplasmic β-catenin protein is constantly degraded by the action of the destruction complex, which is composed of the scaffolding protein Axin, the tumor suppressor adenomatous polyposis coli gene product (APC), casein kinase 1 (CK1), and glycogen synthase kinase 3 (GSK3). CK1 and GSK3 sequentially phosphorylate the amino terminal region of β-catenin, resulting in β-catenin recognition by β-Trcp, and subsequent β-catenin ubiquitination and proteasomal degradation (He et al., 2004). In contrast, the arrival of a Wnt ligand provokes functional inactivation of the destruction complex, resulting into β-catenin accumulation and formation of nuclear complexes with the β-catenin DNA-binding partners TCF/Lef (Clevers, 2006). YAP/TAZ have been demonstrated to be component of the destruction complex and cytoplasmic YAP/TAZ associated to Axin is required for recruitment of β-TrCP to the complex. Thus, in absence of Wnt, depletion of YAP/TAZ leads to the activation of β-catenin/TCF transcriptional responses. Instead, the presence of a Wnt ligand triggers the association between the Wnt receptor LRP6 and Axin with concomitant release of YAP/TAZ from the destruction complex. In this situation, the destruction complex is "invisible" to β-TrCP, avoiding β-catenin degradation and triggering YAP/TAZ accumulation in the nucleus and leading to the activation of Wnt-induced, YAP/TAZ-dependent transcriptional responses (Azzolin et al., 2014). Integration of all these abovementioned inputs (and likely much more) has a role in the determination of YAP/TAZ nuclear levels and transcriptional responses.

YAP/TAZ and Stem Cells

Stem cell activity oscillates throughout an organism's life to maintain homeostasis in all tissues and conditions. As an animal develops and grows, its organs must change and renew themselves according to environmental and physiological stimuli. The Hippo signalling pathway has been implicated as a key regulator of organ size control across species. Mutations in components of this pathway are associated with

overgrowth phenotypes, which are the result of an increase in mitosis and a decreased susceptibility to undergo cell death, and eventual onset of cancer in various tissues (Ramos and Camargo, 2012). Some of these results have been interpreted as a regulation of YAP/TAZ on resident SCs. Anyway, conditional genetic inactivation of YAP in adult mammary gland, pancreas, liver, and even dual knockout of YAP and TAZ in the intestine was largely inconsequential for normal physiology (Azzolin et al, 2014; Chen et al, 2014; Zhang et al, 2010; Zhang et al, 2014). Intriguingly, however, YAP and TAZ are strikingly essential in conditions in which stem cells need to be amplified for tissue regeneration (for example for intestinal crypt regeneration ex vivo) or after oncogenic transformation (in the case of intestinal crypt overgrowth induced by APC deficiency) (Azzolin et al, 2014; Zanconato et al 2015; Yui et al, 2018; Chen et al, 2014; Zhang et al., 2010, Zhang et al., 2014). Other reports also suggested a role of YAP/TAZ in cellular crowding and cell-cell contacts in regulating Hippo signalling, linking cell-cell communication to the physiological needs of organ growth (Chen et al, 2010; Aragona et al, 2013).

The growth of solid tumors has been relied on cells with properties of stem cells, called cancer stem cells (CSCs) (Visvader et al., 2012). TAZ plays a role on endowing cancer stem cell characteristics. In particular, overexpression of TAZ favors proliferation, capacity to resist stress and chemotherapy, and loss of differentiation markers in non-stem cancer cell populations, enabling them to generate high-grade, undifferentiated tumors (Bartucci et al., 2014; Cordenonsi et al., 2011). Moreover, high expression of YAP/TAZ have been associated with the development of breast and lung cancer metastasis both in mice and human (Cordenonsi et al., 2011; Lamar et al., 2012; Lau et al., 2014). These concepts, may suggest a correlation between tumor progression and malignancy, due to a YAP/TAZ-mediated increase in the cancer stem cell pool driving tumor development (Piccolo et al., 2014).

SWI/SNF as epigenetic regulators of chromatin structure

Chromatin structure is regulated by two different classes of complexes that dynamically cooperate to control gene expression. One class comprises complexes that covalently modify histone tails, the other comprise ATP-dependent complexes that are involved in nucleosome remodeling. According to subunit composition and biochemical activity, the second class can be further divided into families such as SWI/SNF, ISWI, INO80, SWR1 and NURD/Mi2/CHD complexes. Among these, SWI/SNF complexes have been found to be specifically inactivated by mutations at very high frequencies in human cancers (Wilson and Roberts, 2011), suggesting a role in tumor suppression.

SWI/SNF chromatin remodeling complexes are a family of evolutionarily conserved multi-subunit complexes, that display multiple functions (Figure 1b). These complexes are found in two major subtypes, BAF and PBAF, that usually include multiple subunits like ATPases that hydrolyze the ATP, or factor essential for binding to DNA or proteins. In humans, three of these subunits (INI1/SMARCB1/SNF5, BAF155/SMARCC1, and BAF170/SMARCC2) are called "core subunits" as they are essential for the ATP-dependent chromatin remodeling activity (Savas and Skardasi, 2018).

These complexes can modulate gene expression by interacting with transcription factors, coactivators, and corepressors, and they can act mobilizing nucleosomes at the level of promoters and enhancers (Hu et al., 2011; Tolstorukov et al., 2013; Yu et al., 2013). They can also be involved in various types of DNA repair (Dykhuizen et al., 2013; Gong et al., 2006; Hara and Sancar, 2002; Park et al., 2006; Watanabe et al., 2014).

SWI/SNF in Cancer

SWI/SNF complexes have been linked to cancer for the first time thanks to the discovery of mutations of SNF5 in rhabdoid tumors (RTs), a rare but highly aggressive pediatric sarcoma (Biegel et al., 1999; Versteege et al., 1998). Snf5 was subsequently validated as a strong tumor suppressor in genetically engineered mouse models (Guidi et al., 2001; Roberts et al., 2002). Later on, genome sequencing studies allow the

discovery that many other types of cancer have SWI/SNF subunit mutations. Several subunits of SWI/SNF complexes (like ARID1A/B, SMARCA 2/4, SMARCB1, SMARCE1, etc.) have been found as recurrently mutated in 20% of all human cancers (Helming et al., 2014; Wilson and Roberts, 2011). The role of mutated SWI/SNF complexes in cancer and the mechanisms behind their related oncogenesis are currently under investigation.

The role of SWI/SNF in lineage specification

SWI/SNF complexes play an important role in lineage-specific differentiation. Several tissue-specific transcription factors cooperate with SWI/SNF complexes during differentiation to coordinate the activation of lineage-specific programs and the suppression of proliferation genes (de la Serna et al., 2006; Flowers et al., 2009; Young et al., 2005).

Mammalian SWI/SNF complexes are highly variable in their composition: in addition to standard core subunits, these complexes contain variant subunits that are specific according to lineages or tissues. It has been reported that hundreds variants of SWI/SNF complexes could exist (Wu et al., 2009).

Analogously, in Embryonic Stem (ES) cells a specific combination of core SWI/SNF subunits and associated factors cooperate to regulate pluripotency and self-renewal. (Gao et al., 2008; Ho et al., 2009; Kidder et al., 2009; Yan et al., 2008). In line with this, inactivation of BRG1 or ARID1A in ES cells leads to their differentiation (Bultman et al., 2000; Ho et al., 2009) and overexpression of the core subunits BAF155 and/or BRG1 in fibroblast causes their reprogramming to induced pluripotent stem (iPS) cells (Singhal et al., 2010). It has also been demonstrated that mouse embryos lacking the SWI/SNF subunits ARID1A, BRG1, SNF5 or BAF155 die at very early stage of development because of an imbalance in the transcriptional regulation (Guidi et al., 2001; Klochendler-Yeivin et al., 2000; Roberts et al., 2000). All these

observations taken together suggest that the SWI/SNF complex plays as a key factor in balancing stem cell self-renewal and pluripotency, and coordinate embryonic development. Moreover, can be proposed that the SWI/SNF mutations can lead to an oncogenic stimulus because of its fundamental role in the regulation of the balance between self-renewal and differentiation.

Organoids

Somatic Stem Cells (SC) operate in multiple adult organs for tissue renewal or repair after damage. The availability of normal, somatic SCs is critical for effective application in regenerative medicine, and for modelling disease (Sato et al., 2013). Somatic SCs have the capability to self expand and initiate morphogenesis in vitro once embedded in matrix facsimiles such as Matrigel, generating complex 3D structures that closely resemble their in vivo counterpart (Sato et al., 2013). These structures, also known as organoids, can be defined as a collection of organ-specific cell types developed from stem cells that are able to self-organize into tissue-like structures, recapitulating the architecture and the growth pattern of the original tissue. Organoids maintain proliferative potential, recapitulate some specific functions of the organs, and are amenable to standard experimental manipulations used for cell lines, including long-term storage by freezing, transfection of DNA and of small interfering RNA, and infection with recombinant viruses (Koo et al., 2012). Organoids can be analysed by standard techniques, such as immunohistochemistry and confocal immunofluorescence, gene expression, mass spectrometry and others. Transgenic alleles, if present, can be easily manipulated in culture and their effects followed in real time. Organoids recapitulate the complete stem cell differentiation hierarchy and allow the in vitro study of cell fate determination. Each organoids model requires a specific medium formulation, in order to provide the right supporting niche factors for stem cell growth.

Organoids in cancer

Cancer still remains, besides few notable exceptions, a largely unmet medical need. Frequently cancer models only poorly recapitulate a patient's tumor, thus initially promising drugs fail in clinical trial, despite good result obtained in vitro (Caponigro et al., 2011). Cancer cell lines from primary cancer tissue are generated with poor efficiency, and they undergo a strong adaptation and selection in vitro. Organoids can be derived with high efficiency from patient-derived healthy and diseased tissue, giving the possibility to use a new and powerful model system to explore cellular and cancer biology. Tumor-derived organoids obtained from diseased pancreas, prostate, bladder, and breast, reflect tumor tissue of origin both phenotypically and genetically (Boj et al., 2015, Gao et al., 2014, Lee et al., 2018, Sachs et al 2018), allowing to explore translational applications including development of early detection method, cancer prevention and personalized medicine. Organoids can be engrafted into murine tissue, maintaining their histopathological features, allowing interrogation of human cancer in complex in vivo environment (O'Rourke et al., 2017, Fumagalli et al., 2018). Organoids can play a fundamental role in new drugs discovery and development, since they are suitable for high-throughput drug screening (Sachs et al., 2018; van de Wetering et al., 2015; Gao et al., 2014), and profiling of patient-derived organoids may reveal causal epigenetic and/or genetic changes that could be used to stratify individual patient to personalized treatment regimens. Generation of organoids from both healthy and tumor tissue generation allows for screening for drugs that specifically target only tumor cells (Drost et al., 2018), and generation of organoids from different region of the same tumor allow to investigate genetic, epigenetic, and transcriptomic profile of different tumor subclones (Fuji et al., 2016, Lee et al 2018). The establishment of organoids from transgenic mouse strains with particular oncogenic transgenes enabled rapid testing of the effects of a particular mutation in context of a specific genetic background (Nadauld et al., 2014), and the recent revolution in genome-editing technologies such as CRISPR-Cas9 also provides a platform to investigate the possibility of correcting gene defects leading to disease (Schwank et al., 2013). Finally, organoids can help to investigate the interaction between tumor cells, ECM and surrounding non-malignant cells types, using

coculture of organoids, stromal cells and other cell types (Katano et al., 2013, Li et al., 2014, Ootani et al., 2009). The complex signalling network so generated can help to establish a supportive niche for tumor growth and could provide novel therapeutic targets.

Nothing was known on SWI/SNF-YAP/TAZ relationship in organoid models. However, previous work of the lab indicated that there is a remarkable overlap between the biological effects of YAP/TAZ activation and SWI/SNF inactivation, including control of cell fate plasticity, gain of stemness properties, gain of organoid forming capacity and tumorigenesis. For instance, in mammary gland cells, loss of SWI/SNF induced organoid forming capacity in a YAP/TAZ-dependent manner (these results were preliminary data already obtained in the lab). We therefore decided to expand these results to liver cancers, using both mouse and human cells.

RESULTS

PART I

In the first part of this thesis, we aim to demonstrate that SWI/SNF chromatin remodeling complex can exert a tumor suppressive functions *in vivo*, in a liver context, by inhibiting YAP/TAZ.

SWI/SNF association to YAP/TAZ: previous background

The results pertaining to this paragraph were obtained in the laboratory and have been published in Chang et al Nature 2018 after I started my project. This paragraph and connected Figure 2 is a summary of the necessary preliminary results with which all the rest of my project was built.

To better understand YAP/TAZ activity regulation, we aimed to identify endogenous YAP/TAZ-binding partners by a proteomic analysis.

Lysates from MCF10A cells stably-expressing Flag-tagged YAP 5SA (a costitutively active form of YAP) and MCF10A cells were subjected to anti-Flag immunoprecipitation. Eluates were run on a 4-12% gradient SDS-PAGE and the gel was sent to the EMBL core proteomic facility for MS analysis. As shown in Table 1, reported YAP-interacting proteins, such as LATS, AMOTL2 and TEAD, were identified, thus validating our experiment. Among all the interactors identified, the association of YAP with several components of the SWI/SNF chromatin-remodeling complex (ARID1A, ARID1B, BRG1, SMARCC1, BAF53a, SMARCA5) was particularly interesting (as highlighted in Table 2). Classical immunoprecipitation experiment validated interaction of YAP to BRG1, BRM, ARID1A, and other SWI/SNF components (such as SNF5 and BAF53a) (Figures 2a, 2b).

To investigate which SWI/SNF component is primarily involved in interacting with YAP, HEK293T cells were co-transfected with Flag-BRG1 and HA-YAP5SA, in absence or presence of independent pairs of siRNAs depleting individual SWI/SNF

components, such as ARID1A, BAF53 or SNF5. Remarkably, only the depletion of ARID1A impaired the ability of BRG1 to associate with YAP (Figure 2c). Similar results were obtained for BRM (Figures 2d). The results indicate ARID1A mediates this association of BRM and BRG1 to YAP (Figures 2e, f).

To assess the functional role of SWI/SNF for YAP/TAZ, we tested on YAP/TAZ activity using YAP-TEAD luciferase reporter (8XGTIIC-Lux reporter) SWI/SNF loss of function in HEK293 cells. Both siARID1A and siBRM increased luciferase reporter activity, indicative for increased YAP/TAZ activity (Figure 2g).

Similarly, inactivation of ARID1A led to YAP/TAZ transcriptional response in MCF10A mammary cells, as measured by the expression levels of YAP/TAZ direct targets like CTGF (Figure 2h). Data presented above predicts a model in which, to fully unleash YAP/TAZ activity, YAP/TAZ nuclear entry should be accompanied by removal of their SWI/SNF-dependent inhibition

ARID1A prevents YAP/TAZ-driven liver tumorigenesis

We next aimed at validating the role of SWI/SNF as nuclear inhibitors of YAP/TAZ a context that is a paradigm for YAP/TAZ biology in vivo, that is, tumor development in the mouse liver (Benhamouche et al., 2010; Camargo et al., 2007; Dong et al., 2007; Yimlamai et al., 2014; Zhang et al., 2010). We first tested this model by fostering nuclear accumulation of YAP/TAZ by liver-specific inactivation of NF2, a Hippo pathway component that promote the assembly of the appropriate protein scaffolds that allow YAP phosphorilation. Liver-specific embryonic knockout of Nf2 leads to YAP-dependent formation of hepatocellular carcinomas (HCCs) and cholangiocarcinomas (CCAs), in adult mice life after long latency (Benhamouche et al., 2010; Zhang et al., 2010). According to our model, we hypothesized that, by keeping YAP/TAZ at bay, SWI/SNF could contribute to the long latency of these tumors. Thus, SWI/SNF removal should accelerate tumorigenic process. To verify this hypothesis, we obtained

mice (LKO=liver conditional knock-out) bearing tamoxifen-inducible CRE recombinase under the control of the hepatocyte-specific Albumin promoter (*Albumin-CRE-ER^{T2}*) (Schuler et al., 2004) and homozygous floxed alleles for *Nf2* and *Arid1a.* Moreover, this mice were crossed together with mice bearing a Lox-STOP-Lox-YFP cassette. This setup allowed us to specifically knockout *Nf2* and *Arid1a* in adult hepatocytes, and to perform parallel lineage tracing. Indeed, all the cells experiencing the Cre recombinase activity (and so the knockout) will also excide the STOP cassette before YFP, leading to a fluorescent tracing of those specific cells.

Homozygous depletion of *Nf2* from adult hepatocytes caused the appearance of ductular reactions around the portal area within 4 months, characterized by the presence of small cells with scant cytoplasm (called oval cells) (Figure 3a). These ductular reactions were rare: in Nf2 LKO mice, 10,4±0,8 % of portal spaces per section presented ductular reactions (n= 7 analyzed animals with 3 different sections per animals), despite quantitative *Nf2* deletion had occurred in the liver parenchyma (Figure 3d). These lesions were almost inert, with few Ki67 (a cellular marker for proliferation) positive cells and no sign of cellular atypia, and remained confined to the portal areas up to 4 months after tamoxifen administration in all *Nf2* KO mice (n=7) (Figures 3a-b). On the molecular level, oval-like cells expressed the ductal markers pan-cytokeratin (panCK, a marker widely used for oval cells identification, but also for tumor characterization) (Figures 3c and 3e) and displayed nuclear staining for both YAP and TAZ (Figures 3f-g); moreover, YAP nuclear staining could be detected in periportal hepatocytes of *Nf2* LKO, but not in hepatocytes from control mice, which display cytoplasmic YAP (Figure 3f). In spite of increased nuclear YAP/TAZ localization induced in a number of cells in *Nf2* LKO, YAP/TAZ transcriptional activity was only modestly induced when compared to control, as measured by *Ctgf*, *Cyr61* and *Ankrd1* expression at the four months time point (Figure 4a). These results

demonstrate that Nf2 depletion in the liver is not able to induce tumorigenesis in a short period of time.

The combined knockout of *Nf2* and *Arid1a*, instead, had a dramatic effect. All *Nf2/Arid1a* LKO mice exhibited an impressive liver overgrowth four months after Cre activation (Figures 4b and 4c), with widespread areas of neoplasia, ranging from early ductular atypia to full-blown cholangiocarcinomas, mostly constituted by oval-like, cytokeratin-positive cells pervasively infiltrating the surrounding parenchyma (Figures 3a, 3c and 3e). In addition, HCC developed at this stage in all the double mutants (n=7) (Figures 3a-c), whereas no tumors were ever observed in any *Nf2* LKO at the same stage (n=7). An extensive degree of proliferation was evident in lesions and all across the remaining hepatocytes, as revealed by Ki67 staining (Figure 3b). Remarkably, YAP/TAZ activity was massively activated in *Nf2/Arid1a* mutant livers that displayed a 50-100-fold increased mRNA levels of *Ctgf* and *Ankrd1*, when compared to *Nf2*- or *Arid1a*-only mutant livers (Figure 4a). By lineage tracing with R26-LSL-YFP both HCC and intrahepatic CCA were YFP-positive, indicating that both types of lesions originated from hepatocytes (Figure 3e). The knockout of *Arid1a* alone had only minimal effects, with ostensibly normal livers displaying only rare Ki67-positive nuclei, and no significant alterations within the ductal plate (Figure 3a-c). Intriguingly, we observed that combined *Nf2/Arid1a* LKO also displayed hundreds-fold induction of *Afp* (Figure 4a), a marker of fetal hepatoblasts, that was never detected in individual *Nf2* or *Arid1a* mutants. Expression of *Afp* was also noted in the liver of transgenic mice overexpressing exogenous YAP (Yimlamai et al., 2014), inferring that the elevated level of endogenous YAP activity in *Nf2*/*Arid1a* LKO might trigger the reprogramming of hepatocytes to a more primitive, progenitor state. Overall, data suggest that the combination of aberrant Hippo signaling and attenuation of SWI/SNF activity through ARID1A inactivation potently enables YAP transcriptional responses fostering conversion of hepatocytes into tumor-initiating liver progenitors (Figures 4a and 3a-c).

We also wanted to functionally validate the requirement of YAP/TAZ in this setup. We discarded the strategy of genetic YAP/TAZ conditional knockout concomitant to Nf2/Arid1a knock-out due to very complicated crossings and genotypes. We instead decided to pursue the following experiments: 1) treatment of Nf2/Arid1a liver conditional knock-out mice with the YAP/TAZ inhibitor verteporfirin; 2) YAP/TAZ-mediated knock-down in tumor organoids derived from fully established tumors developed by Nf2/Arid1a liver conditional knock-out mice.

As for the former part, we treated *Albumin-CRE-ER^{T2}; Nf2 fl/fl; Arid1a fl/fl* mice treated with tamoxifen. After two 2 months, we administered to the mice Verteporfirin, a drug clinically used in photodynamic therapy for neovascular macular degeneration proven to be a suppressor of YAP–TEAD complex (Feng et al., 2016) . However, this treatment was not able to rescue the cancerous phenotype. We suggest that this result can be related to the timing of the experiment: waiting 2 months for the administration of verteporfin after tamoxifen injection could be too late, as the phenotype caused by Nf2/Arid1a depletion is already too severe to be rescued by this drug. Regarding the experiment of YAP/TAZ knock-down in organoids, this strategy allowed us to demonstrate in vitro the requirement of YAP/TAZ for the formation of tumor organoids deriving from Nf2/Arid1a-depleted liver, as such establishing a fundamental role of YAP/TAZ downstream to these genetic insults (see Figure 7 and page 19 for details).

To further extend these investigations we also tested whether ARID1A inactivation could foster tumor initiation through activation of endogenous YAP/TAZ, even in the absence of genetic lesions (such as NF2) directly leading to YAP activation. In mouse models continuous rounds of liver injury and subsequent compensatory proliferation are implicated in cancer initiation and promotion: for this reason, we decided to investigate the consequences of ARID1A inactivation in a context of regenerating liver. To do this, we induced chronic liver damage through dietary addition of the toxic compound 3,5-diethoxycarbonyl-1,4-dihydrocollidine (DDC, Figure 5a). We

administrated DDC diet to the mice for 6 weeks, and then we collected and analyzed the livers. Chronic DDC exposure turned on YAP/TAZ activity as monitored by the expression of gene signatures for YAP/TAZ activities in mouse liver (Figure 5b). By histological examination, DDC treatment caused ductular reactions in control livers in which keratin-positive oval cells appearing around the portal areas (Figure 5c-d). These results were similar to what we observed previously in Nf2 depleted liver, suggesting that Verteporfin treatment, and thus chronic liver injury, could resamble a genetic lesion. Strikingly, however, in *Arid1a* LKO mice, areas of cholangiocarcinomatous transformation were clearly evident in all examined mice (n=10) (Figure 5c-d), accompanied by increased level of *Afp* expression (Figure 6a); clear signs of atypia and proliferation were present in these lesions (Figures 5e). Crucially, these lesions were absent in the DCC-treated cohort in which liver-specific *Arid1a* deletion was combined to YAP/TAZ inactivation (n=15); in these triple *Arid1a/Yap/Taz* mutant livers, histology and *Afp* expression was similar to control DDC-treated mice (Figures 5c-e and 6a). Most of DCC-treated/ARID1A mutant livers later evolved into full-blown cholangocarcinomas characterized by desmoplastic fibrotic reaction surrounding the ductular structures (Figure 6b). In the context of the fibrotic tissue, rare CK positive tumor cells could be detected infiltrating the stroma (Figure 6b, middle columns). Importantly, simple withdrawal of DDC food was not able to rescue the phenotype, but concomitant inactivation of YAP/TAZ in triple *Arid1a/Yap/Taz* LKO mice completely prevented the emergence of any lesions (Figure 6b, last columns), highlighting how inhibition of YAP/TAZ is an essential mediator of SWI/SNF tumor suppressive properties.

All these data together demonstrate that ARID1a display a tumor-suppressing role sequestrating YAP/TAZ, thus preventing YAP/TAZ-driven liver tumorigenesis.

Yap/Taz requirement in Arid1a-driven tumorigenesis in mouse liver organoids

Since organoids are emerging as a promising technology to reproduce phenotypically and genetically the tissue of origin in culture, this model attracted our attention as suitable culture system to address biological questions that remain unanswered in in vivo set ups, such as the YAP/TAZ requirement for the lesions developed by Nf2/Arid1a liver conditional knock-out mice.

We treated *Albumin-CRE-ER^{T2}; Nf2 fl/fl; Arid1a fl/fl* mice with intraperitoneal injection of tamoxifen and wait for tumor development. After 4 months, livers exhibited overgrowth, and tumor masses, as described above. Liver biopsies were finely minced, digested with collagenase type I and plated in 100% Matrigel (Huch et al., 2013, Table 3) with a medium containing cytokines such as Epithelial Growth Factor (EGF), Hepatic Growth Factor (HGF) and Fibroblast Growth Factor 10 (FGF10), sustaining liver organoids growth. Cyst-like organoids started to grow after 24 hours, letting us to establish an organoid culture. The conditions favoring this expansion however does not discrimitate between tumor organoids and normal bile duct organoids: as such, our first isolation and expansion lead to a mixed culture of normal (diplaying *Nf2* and *Arid1a* floxed alleles) and tumor (*Nf2* and *Arid1a* knockout alleles) organoids. To overcome this problem, we adopt a clonal expansion strategy: single organoids were hand-picked for clonal growth and each clone was subjected to genomic DNA extraction and PCR. Only clones displaying *Nf2* and *Arid1a* knock out alleles were selected for further expansion and studies (Figure 7a). Tumor organoids were extracted from Matrigel, digested at single cells, and transfected with siControl or siYAP/TAZ according to the organoid lipofection protocol (see Methods for details). Organoids transfected with siControl reformed round-shaped organoids after seeding; in contrast organoids depleted of YAP/TAZ remained at single cells level (Figure 7b). This demonstrated that YAP/TAZ are required for propagation of organoids derived from tumor generated from Nf2/Arid1a depleted mouse liver, but not for propagation

of normal organoids. We can conclude that YAP/TAZ have a fundamental role in tumorigenesis driven by N2 and Arid1a knock-out.

Establishment of organoid cultures from healthy and tumor human liver biopsies

Mutations leading to inactivation of SWI/SNF components have been identified at exceedingly high frequency in a variety of human malignancies, suggesting a widespread role for SWI/SNF in tumor suppression (Helming et al., 2014; Kadoch and Crabtree, 2015). In parallel to our work on mouse models, we next aimed to investigate the role of SWI/SNF complex in human cancers. We again decided to focus our attention on adult liver, because mutations in SWI/SNF complex components, in particular ARID1A, are frequent in human cholangiocarcinomas (Jiao et al., 2013). Our aim was therefore comparing healthy liver vs cholangiocarcinoma organoids derived from the same patient when possible.

Following ethical agreement, we enrolled several cholangiocarcinoma (CCA) patients that did not received any neo-adjuvant therapy before surgery, thanks to a collaboration with the Hepato-biliary Surgery Unit of Azienda Ospedaliera di Padova (Prof. Cillo team). From the resected liver area of each patient, we collected one biopsy from tumour area and one from healthy area (as far as possible from the tumor site). From each biopsies, we saved a small piece of tissue to confirm by histological analysis its tumor/healthy nature, and from the remaining tissue we tried to establish organoid cultures.

To do this, liver biopsies were first manually minced with surgical blades (part of the sample was preserved as frozen stock), and then digested with Collagenase type I in different concentrations according to the tissue stiffness, in order to isolate single cells. If necessary, the samples were also treated with haemolytic solution to eliminate red blood cells. The suspension was filtered through a 70 µm Nylon cell strainer, spun down, re-suspended in 100% Matrigel, and plated in low-attachment plate. After

Matrigel has formed a gel, Liver Organoids Expansion Medium (Table 3) was added, to allow the expansion of ductal organoids after 1-2 days. The successs rate of organoid preparation depended on the amount of starting material. As such, it is impossible to provide an estimate of the number of organoids growing from each patient. However, from each patient we always obtained outgrowths that could be further passaged. Organoids from both healthy and tumor liver biopsies self-organized into a single layered structure that displayed a round, empty cyst-like shape (Figure 8a), as confirmed by haematoxylin and eosin staining (Figure 8b).

Since self-renewal potential is one of the peculiar characteristics of stem cells, we tested if the organoids retained this capability. Organoids were harvested from Matrigel, enzymatically dissociated to single cells, and re-plated in the same conditions. After dissociation, new organoids grow up in few days, demonstrating that cells inside the organoids retain self-renewal capability. This procedure was repeated for many times (even 15), demonstrating that organoids can be passaged through various generations, remaining in culture for even 2-3 months, without any visible morphological change (Figure 8c). So far, we were able to enrolled 7 patients, and we succeed in establishing organoid cultures from all of them.

To validate our model, we decided first to verify how close our organoids recapitulate the tissue of origin, testing the tumor forming capability of these cells in vivo. Subcutaneous injection of organoids in 100% Matrigel were performed in NOD/SCID mice. The experiment was performed both for healthy and tumor organoids, in the presence or absence of human fibroblast (BJ cells) transformed with an active form of YAP, in order to create an environment prone to tumor formation, mimicking CCA fibrotic stroma. We opted for this solution because it has been demonstrated that co-culture of organoids and fibroblast can increase organoid proliferative ability (Koledova et al., 2017; Hegab et la., 2015) and that stroma can display either tumor-suppressing or tumor-promoting abilities. In particular the Tumor Reactive Stroma

(TRS) is a defined environment composed by several cell types, among which cancer-associated fibroblasts (CAF) secrete high levels of TGF-beta, IL-6, SDF-1, EGF, and FGF, able to sustain cancer cells growth. CAFs may also release several Metalloproteinases (MMPs), able to trigger EMT by cleaving cell adhesion molecules on the surface of cancer cells (Brivio et al., 2017; Cirri et al., 2011). Moreover, it has been shown that altered expression of Yap in cholangiocarcinoma, may promote EMT (Pei et al., 2015).

Transplanted animals were monitored visually. In the month following injections, tumor masses grew and expanded only when tumor organoids in combination with fibroblast were transplanted: however, after this first period of growth, the same masses underwent regression till they almost disappear. After 1 or 3 months from the subcutaneous injections, we collected remaining very small masses, however histological analysis did not reveal tumor presence (Figure 8d). Masses never grew from transplanted normal bile duct organoids.

To understand why the organoids that we isolate were apparently not tumorigenic, we decided to perform a gene expression profiling by RNA-seq of our organoids. The comparison between tumor and healthy organoids did not reveal differences between the two populations, suggesting that what we considered a tumoral organoid population was actually composed by healthy cells. We conclude that our in vitro conditions were not able to mimic the proper context of tumor organoid growth. We are currently unable to discriminate whether our conditions select expansion of contaminant healthy cells- into organoids, or if the culturing conditions in fact revert CCA cells into normal ones (see Discussion).

In conclusion, the establishment of human cholangiocarcinoma organoids culture, remain a critical step, that needs to be improved, exploring other possibilities to find the right environmental context for tumor organoid expansion.

PART II

In the second part of this thesis we want to characterize early colonies arising from LD cells after YAP transfection (as described in Panciera et al., 2016), in order to dissect which mechanisms are triggered by YAP transformation.

YAP/TAZ mediated reprogramming in mammary gland: previous background

Recently in our laboratory, we have reported that expression of YAP in primary, terminally differentiated cells (LD) of the mouse mammary gland mediates conversion to mammary stem-cells indistinguishable from normal, naturally-born SCs (MaSCs) (Panciera et al., 2016). This reprogrammed population was named YAP-induced MaSCs (yMaSCs). This procedure is based on the FACS purification of LD cells (positive for luminal markers like K8, K18, K19) and their following conversion into yMaSCs by YAP expression. yMaSCs initially grow as colonies, but has also been established a protocol for their long-term propagation as organoid, a system that preserve their stem properties like self-renewal and differentiation.

YAP/TAZ role in dedifferantion

We focused our attention on the characterization of the initial phase of reprogramming, carrying out Immuno-Fluorescent (IF) analyses on the earliest yMaSCs emerging as colonies from YAP-expressing LD cells. Surprisingly, difference to organoids, we found that a large fraction of these colonies consists of cells double positive for the basal K14 and the luminal K8; in contrast, colonies were virtually lacking staining for the myoepithelial marker alpha-SMA (Figures 9a-c). This indicates that the early yMaSCs do not represent a transdifferentiation of LD into myoepithelial cells; rather, the early yMaSCs appeared to represent a transitional state between LD and MaSCs cells, in particularly a progenitor-like state distinct from those prevalently found in the

adult mammary gland and reminiscent of embryonic/fetal mammary progenitor cells, that are indeed double K14/K8-positive and alpha-SMA negative.

To get more insights on the nature of early yMaSCs, we compared RNA-seq analyses of early yMaSC colonies, to control LD and MaSC-enriched basal cell populations just sorted from the mammary gland. As shown in Figures 8d-e, the LD-to-yMaSC transition triggers downregulation of a group of luminal genes highly expressed in terminally differentiated cells (e.g., *Estrogen Receptor* and *Wap*, see blocks A-B in Figure 8d) and upregulation of a host of basal markers originally not expressed in LD cells (including *K14, K5, ΔNp63, LGR4* and others, see block F in Figure 9d). In contrast, other markers remain repressed in early yMaSCs, including myoepithelial markers such as *Myh11, Calponin1, Mrtf-a, Myosin-light chain kinase* and *Cd10*, as well as *Procr*, recently identified as an adult MaSC marker (Wang et al., 2015) (blocks D-E, see also qRT-PCR validations in Figure 9e). This further reinforces the conclusions that YAP does not induce transdifferentiation of LD into myoepithelial cells. Interestingly, a specific group of genes is exclusively induced in early yMaSCs (block G), and a significant fraction of these (61%) corresponds to genes also expressed in the fetal mammary gland. In line, a significant fraction of the luminal genes (54%) whose expression is retained by early yMaSCs (block C) represents genes also expressed by the fetal mammary gland. Altogether, this is consistent with early yMaSCs representing a cellular state that is distinct from adult progenitors but instead shares molecular features of multipotent fetal mammary progenitors. As such, we can conclude that with our procedure (YAP induction together with culture conditions) we can capture a mammary cellular state that in vivo the cells experienced only during development, and in particular during the phase of fetal mammary gland. We then asked whether this fetal cellular state was stable during time and culture conditions. Interestingly, we noted that the fetal state of yMaSCs is only transient, as when yMaSCs were transferred in organoid medium they readily matured into cells

displaying a profile matching adult MaSC-enriched populations, that, as shown in Figure 8f, express myoepithelial and basal marker without co-expression of luminal genes.

Generation of human mammary tumor organoids

After having set up the organoid culture conditions for mouse normal mammary gland (Panciera et al., 2016) we aimed to culture and expand organoids from human primary tumors. In collaboration with the mammary oncology team of Istituto Oncologico Veneto (IOV), breast cancer patients candidate to surgical resection but naïve to any other treatment were enrolled in this explorative study and asked to donate a small amount of the tumor to our Laboratory in order to be processed for organoid derivation. All the procedures were approved by the Ethic Committee of IOV.

During the months of this Thesis we obtained 5 mammary tumor samples: 2 triple-negative breast cancers and 3 HER2-positive breast cancers, as indicated in Table 4. HMaTu_001, a triple negative breast cancer, was digested with the same conditions described above for normal mouse mammary gland (digestion with colloganase + hyaluronidase, at 37°C) for 3 hours. We indeed noticed that, compared with mouse normal mammary gland, tumors in general are stiffer (because of an intense desmoplastic reaction, characterize by a pervasive growth of fibrous tissue) and required a longer dissociation time (even overnight). After digestions, the sample was composed by: some debris (mainly collagen fibers or calcifications), single cells, grapes/groups of cells organized into epithelial-like structures, and undissociated clamps (Figure 10a). All these were centrifuged, washed, resuspended in 100 % cold Matrigel and seeded in wells of a 24-well ultra-low attachment plate. After Matrigel formed a solid gel, medium 1 enriched in cytokines like EGF and bFGF (see Table 4) was added and the growth/expansion of organoids was monitored daily. Rock inhibitor Y27632 was added to the medium only during the first 3 days of culture, because of its

pro-survival effects on dissociated stem cells (Watanabe et al., 2007). Generally, organoids grew better and faster from the multicellular epithelial-like structures present at the moment of seeding. Primary organoids (i.e. organoids formed after the initial dissociation) grew surprisingly fast (2-3 weeks) and the bigger ones reached dimensions in the sub millimetre range, clearly visible also at naked eyes. Their visible day-by-day growth was a clear effect of proliferation (Figure 10b). Prompted by the experience with mouse organoids, we decided to passage these organoids (too few in any case to be processed for further analysis). We therefore harvested HMaTuORG_001 from Matrigel, and decided to either fragment them by mechanical pipetting or digest them with trypsin at the single cell level (20 minutes, with intermediate pipetting). In both conditions, cells were re-seeded in 100% Matrigel + medium 1. With both strategies, however, we were unable to obtain the desired expansion: the fragmented replated organoids remained as such and eventually died, whereas from the single-cell dissociated organoids no outgrowths re-appeared. This lack of culture expansion was repeated for HMaTuORG_002, derived from a HER2-positive breast cancer, with growing primary organoids but unable to be propagated after dissociation/replating (Figure 10c). In particular, for HMaTuORG_002 we combined a culture media enriched with EFG, Noggin and R-Spondin (ENR) with treatment with the ovarian hormones oestrogen and progesterone. Indeed, it has been demonstrated that mouse mammary stem cells are highly responsive to steroid hormone signalling; ovariectomy markedly reduced MaSC number and outgrowth potential *in vivo*, whereas MaSC activity increased in mice treated with oestrogen plus progesterone (Asselin-Labat et al., 2009). However, none of these conditions are permissive for passaging/expansions of HMaTuORG_002.

We therefore reconsidered again our culture conditions and critically examined other conditions in order to find a special ingredient to add to the basic EGF/Noggin/R-Spondin (ENR)-based organoid medium. To do this, HMaTu_003 was dissociated, and

HMaTuORG_003 were seeded in 100% Matrigel overlaid by classic ENR medium, or ENR medium added with N-acetyl cysteine (according to Diehn et al., 2009 an anti-oxidant environment is permissive for many stem cell and cancer stem cell niche (Diehn et al., 2009), or ENR+ Cholera toxin/Insulin (these two cytokines are common supplements for breast cancer cell lines, like MCF10A, to stimulate cells growth and increase the time the cells can be subcultured (Stampfer et al., 1982).

The growth of HMaTuORG_003 was in general very slow, and in all conditions, no differences were clear and expansion, measured by the capacity to regrow after passaging, remained an unsolved problem. While HMaTu_004 never generated any primary organoid, with HMaTu_006 we were able to culture primary organoids in Matrigel 100% overlaid by a medium used by Rajagopal and collegues (Mou et al., 2016), with little modifications, containing 10µM ROCKi, A-83-01 5µg/mL, Noggin, and 3µg/mL CHIR99021 and after three weeks mechanically dissociated them and replated in the same conditions. As previously, re-growing after passaging was not efficient.

Again, like for human liver organoids, probably we are able to capture the right environment to allow the growth of our organoids. These results reflect how mouse models do not completely capture human complexity, and how mimic in vitro the right environment that allow organoids to growth.

DISCUSSION

In the data presented in the first part of the thesis, we describe several evidences that confirm our previous studies on SWI/SNF-mediated nuclear inhibition of YAP/TAZ.

In our laboratory, it has been demonstrated that to fully activate YAP/TAZ, at least two checkpoints need to be controlled: stimulation of YAP/TAZ nuclear localization and removal of their SWI/SNF-dependent inhibition.

Here we show that, in mouse liver, SWI/SNF restricts YAP/TAZ activity induced by genetic insults given by Nf2 depletion. Indeed, only the concomitant deletion of both Nf2 and Arid1a leads to massive YAP/TAZ activation, evident by target gene expression, liver overgrowth and tumor formation.

We also confirmed in vitro, taking advantage of organoids propagation technology, that YAP/TAZ are required for SWI/SNF-driven tumorigenesis, as YAP/TAZ depletion prevent tumor organoid growth.

We also noticed that combined *Nf2/Arid1a* LKO displayed massive expression of the hepatoblast marker Afp. We speculate that the high activity of endogenous YAP induced by these genetic modifications leads to hepatocytes reprogramming to a more primitive state.

Then, we demonstrated that a chronic liver injury concur to liver tumorigenesis if concomitant SWI/SNF inactivation is induced. In this set up, we were also able to test genetically the effect of YAP/TAZ requirement for tumorigenesis: indeed, when YAP/TAZ were also depleted in liver of mice treated with DDC and lacking Arid1a , these mice did not developed any tumor.

We hope that our results can be a starting point in dissecting SWI/SNF role as tumor suppressors: indeed, as suggested in literature, a lot of different human tumors display inactivating mutations of different SWI/SNF components, suggesting a role of SWI/SNF in tumor suppression (Helming et al., 2014; Kadoch and Crabtree, 2015).

Interestingly, Arid1a mutation in murine colon lead to carcinogenesis (Guan et al.,

2014), but also mutations in other SWI/SNF components like BRM result in overgrowth phenotype (Reyes et al., 1998), resembling the effects of YAP/TAZ activation.

These conclusions offer the chance to explore new therapeutic possibilities in cancer, as SWI/SNF loss-of-function mutations impact on YAP/TAZ activity and could be potentially controlled by modulating YAP/TAZ.

Despite growing mouse tumor organoids is feasible and quite easy, when we tried to optimize a protocol to isolate and expand human tumor organoid, we were not able to succeed. In the case of CCA, even if at histological examination the samples from which we isolated organoids were ostensibly entirely composed of tumor cells, in our culture condition we were able to propagate and expand only what appeared as normal-like organoids, self renewing like normal organoids from bile ducts, and unable to induce any tumor outgrowth in vivo. One possibility is that the environment that we tried to re-create in vitro (Matrigel as tridimensional support and cocktails of cytokines and growth factors in the medium) allow and sustain the proliferation of healthy cells, causing their unique expansion. Or that the same conditions are in fact counterselecting tumor cell proliferation. Alternatively, what we expand may in fact represent tumor cells "normalized" or epigenetically reprogrammed back into normal-like cells. We have not carried out genome sequencing of our organoids in part for ethical limitations on the genomic informations of the patients at the time of these analyses, in part because CCA has no established genetic drivers, rendering the use of mutations as hallmark of cancer cells essentially impossible, or as finding a needle in a haystack with no comparison possible with the healthy tissue from the same patient.

In the second part of this work, we focused our attention on another system, the mammary gland. Previously in our laboratory has been demonstrated that YAP/TAZ are required to sustain the expansion of primary MaSCs in vitro, and that the expression of YAP/TAZ may confer stemness characteristics also to normal mammary luminal

differentiated cells, converting them into YAP-induced Mammary Stem Cells (yMaSCs) (Panciera et al., 2016). This procedure comprises: 1) the purification by FACS of luminal differentiated cells (LD, positive for luminal markers like K8, K18, K19); 2) the conversion by YAP expression of LD to yMaSCs during a phase in which they grow as colonies; 3) the long-term propagation of yMaSCs (including their cardinal properties of self-renewal and differentiation) as organoids.

We decided to characterize the nature of the early colonies obtained from LD cells with YAP expression, in order to dissect their identity to better understand which is the mechanism behind YAP reprogramming.

We found, by immunofluorescence and by RNA-seq, that yMaSC colonies express marker like K8, K14 and other basal markers originally not expressed in LD cells, while the expression of alpha-SMA and of other terminally differentiated genes is repressed.

A specific group of genes exclusively expressed in early yMaSCs, turned out to correspond to genes expressed in the fetal mammary gland. This means that with our procedure we are able to induce and capture a particular cellular state that is different from adult progenitors and also do not represent transdifferentiation of LD into myoepithelial cells, but that shares molecular features of multipotent fetal mammary progenitors.

Again, we tried to move to a human model system, starting to optimize culture conditions for mammary tumor organoid growth. In this case, we were not able to find the correct combination of elements that allow organoids to be passaged and to propagate over time.

We also tried a recently published protocol (Sachs et al 2017) in which they claim a good rate of success in the establishment and expansion of breast cancer organoids. However, the results coming from these conditions are still under investigation and it is clear that anyway this remains an artisanal technology in need of effective standardization and optimization of the right environment to supply these adult stem cells all the necessary conditions to expand. It is also worth mentioning that such

publication offers minor evidences on the real tumorigenicity of breast cancer organoids, only at the level of "proof of principle" experiments. It is thus possible that also normal tissue is propagated in the same conditions. Moreover, our difficulties in the propagation of such organoids might be consistent with the lack of a proper environmental supply, still to be fully elucidated at the cellular and the extracellular level.

METHODS

The methods here listed are part of the Piccolo lab protocol book and are thus presented with minor modifications, if any, in respect to published material or other thesis work published by our laboratory.

Reagents and plasmids

Doxycycline hyclate, fibronectin, insulin, dexamethasone, dispase, hyaluronidase, NH_4Cl, tamoxifen and 4-OH-tamoxifen were from Sigma. Growth-factor reduced Matrigel was from Corning. Murine EGF, murine bFGF, human Noggin were from Peprotech. B27, Collagenase type I, DMEM/F12 and trypsin were from Life Technologies. R-Spondin1 was from Sino Biological. Rat tail collagen type I was from Cultrex. DNaseI was from Roche.

GFP- and Cre-expressing adenoviruses were from University of Iowa, Gene Transfer Vector Core.

HA-hYAP5SA, was generated by PCR from the original vector cDNAs kindly provided by Dr. Guan (as in Aragona et al., 2013) and subcloned in pBABE retroviral plasmids to establish stable cell lines. pBABE-Puro empty vector was used as control retroviral transduction.

pCS2 Flag-BRG1 was obtained by subcloning Flag-BRG1 from pBABEpuro Flag-BRG1 (Addgene #1957) into pCS2;

For inducible expression of YAP, cDNA for siRNA-insensitive Flag-hYAP1 wt was subcloned in FUW-tetO-MCS, obtained by substituting the Oct4 sequence in FUW-tetO-hOct4 (Addgene #20726) with a new multiple cloning site (MCS). This generated the FUW-tetO-wtYAP used throughout this study. FUW-tetO-EGFP plasmid was used as controls, as previously indicated (Cordenonsi et al., 2011).

All constructs were confirmed by sequencing.

Cell lines and treatments

MCF10A were cultured in DMEM/F12 (Gibco) with 5% horse serum (HS), glutamine and antibiotics, freshly supplemented with insulin (Sigma), EGF (Peprotech), hydrocortisone (Sigma), and cholera toxin (Sigma). HEK293 or HEK293T cells were from ATCC and were cultured in DMEM (Gibco) supplemented with 10% fetal bovine serum (FBS), glutamine and antibiotics.

RNA interference

siRNA transfections were done with Lipofectamine RNAi-MAX (Thermo Fisher Scientific) in antibiotics-free medium according to manufacturer instructions. Sequences of siRNAs are provided in Table 5.

Western blot

Cells were harvested in Lysis Buffer (50 mM HEPES (pH 7.8), 100 mM NaCl, 50 mM KCl, 1% Triton, 5% Glycine, 0.5% NP40, 2 mM $MgCl_2$, 1 uM DTT, phosphatase and protease inhibitors) and lysed by sonication. Extracts were quantified with Bradford method. Proteins were run in 4-12% Nupage-MOPS acrylamide gels (ThermoFisher) and transferred onto PVDF membranes by wet electrophoretic transfer. Blots were blocked with 0.5% non-fat dry milk and incubated overnight at 4°C with primary antibodies. Secondary antibodies were incubated 1 hour at room temperature, and then blots were developed with chemiluminescent reagents. Images were acquired with Image Quant LAS 4000 (GE healthcare).

For Western blot: anti-YAP/TAZ (sc-101199), anti-BAF53a (sc-137062 or sc47808), anti-BRG1 (sc-10768 or sc-17796), anti-SNF5 (sc-166165), anti-ARID1A (HPA005456) and anti-SNF5 (HPA018248) were from Sigma; anti-YAP (ab52771), anti-TAZ (HPA007415) and anti-BRM (ab15597) were from Abcam; anti-GAPDH

(MAB347) and anti-ARID1A (04-080) monoclonal antibody were from Millipore. Horseradish-peroxidase-conjugated anti-Flag (clone M2, A8592) was from Sigma and the anti-HA (A190-107P) was from Bethyl.

Coimmunoprecipitation of Tagged proteins

Cells were harvested and lysed by sonication in Lysis Buffer (50 mM HEPES (pH 7.8), 100 mM NaCl, 50 mM KCl, 1% Triton, 5% Glycine, 0.5% NP40, 2 mM $MgCl_2$, 1 uM DTT, phosphatase and protease inhibitors) and extracts were cleared by centrifugation at 4°C. Extracts were incubated three hours at 4°C with anti-Flag resin (Sigma). Immunocomplexes were then washed with cold Lysis buffer three times, resuspended in SDS sample buffer, and subjected to SDS-PAGE and Western blot analysis. Inputs were loaded according to Bradford. In particular, for Figure 2c, we used lysates from HEK293T cells transfected with the indicated plasmids Flag-BRG1 was 83 ng/cm ^{2}, HA-YAP5SA was 17 ng/cm^2) and harvested 48 hours after transfection.

Mass Spectroscopy

Samples for Mass Spectrometry (MS) were prepared as in (Enzo et al., 2015) starting from 50% confluent cultures of control or Flag-YAP5SA-expressing MCF10A cells. Briefly, cells were harvested in lysis buffer and immunoprecipitations were carried out as described above with agarose-conjugated FLAG M2 antibody (Sigma) for 2.5 hours at 4°C on a rotator. After three washes in the same buffer, immunopurified proteins were eluted by adding 3xFLAG peptide (Sigma) for 30 min at 4°C. Eluates were run in a 4-12% gradient SDS-Page acrylamide gel (ThermoFisher) and the gel was stained with Colloidal Coomassie and then sent to the EMBL core proteomic facility for MS analysis. Each sample lane was cut into five pieces according to molecular weight, and all the proteins contained in each piece subjected to in-gel tryptic digestion. The

resulting peptides were purified and subjected to identification based on their mass according to EMBL parameters.

Identification of native YAP/TAZ complexes by Mass Spectroscopy

Live cells were cross-linked with 1% formaldehyde (Sigma) in culture medium for 10min at room temperature before harvesting. Lysis was achieved by consecutive incubations in Lysis Buffer 1 (50mM HEPES, pH7.5, 10mM NaCl, 1mM EDTA, 10% Glycerol, 0.5% NP-40, 0.25% Triton X-100), Lysis Buffer 2 (10mM Tris-HCl pH8, 200 mM NaCl, 1mM EDTA, 0.5 mM EGTA) and Lysis Buffer 3 (10mM Tris-HCl pH8, 200 mM NaCl, 1mM EDTA, 0.5 mM EGTA, 0.1% Na-deoxycholate, 0.5% N-lauroylsarcosine), followed by sonication with a Branson Sonifier 450D. Immunoprecipitation was performed by incubating cleared extracts (corresponding to $2x10^6$ cells) with 20 µg of antibody (anti-YAP: EP1674Y, Abcam; anti-TAZ: HPA007415, Sigma; pre-immune rabbit IgGs: I5006, Sigma) and 100 µl of Dynabeads-ProteinG (Invitrogen). After extensive washing, immunoprecipitates were eluted in 7.5%SDS, 200mM DTT and de-crosslinked. After alkylation with iodoacetamide (IAA), proteins were purified with SP3 beads as previously described (PMID 25358341), resuspended in 50 mM ammonium bicarbonate and digested with trypsin. Peptides were subjected to SP3 cleanup and they were eluted in 0.1% TFA. Samples were analyzed on an Orbitrap Fusion mass spectrometer (Thermo Fisher). Results are shown in Table 1 and 2.

Quantitative Real-Time PCR

Cells were harvested by RNeasy Mini Kit (Qiagen) for total RNA extraction, and contaminant DNA was removed by DNase treatment. Total RNA from livers and mammary colonies or organoids was extracted using TriPure (Roche). qRT-PCR analyses were carried out on retro-transcribed cDNAs with QuantStudio5 (applied

Biosystems, ThermoFisher Scientific) and analyzed with QuantStudio Design & Analysis software. Experiments in cells were performed at least three times, with duplicate replicates. Expression levels are always given relative to *GAPDH*. PCR oligo sequences are listed in Table 6.

RNA sequencing

For RNA-seq, total RNAs was extracted with Trizol from livers of untreated or DDC-fed (6 weeks) mice and from small colonies emerging from YAP-reprogrammed LD cells after 13 days in mammary colony medium and from freshly sorted LD and MaSC-enriched cell populations. RNA-seq libraries were prepared with TruSeq Stranded Total RNA with Ribo-Zero GOLD (Illumina), according to manufacturer's instructions. Sequencing was performed on an Illumina HiSeq 2500 platform. Raw reads were aligned using TopHat (version 2.0.5) to build version mm9 of the mouse genome. Counts for UCSC annotated genes were calculated from the aligned reads using HTSeq (version 0.6.0). Normalization and differential analysis were carried out using edgeR package and R (version 3.0.0). Raw counts were normalized to obtain Counts Per Million mapped reads (CPM) and Reads Per Kilobase per Million mapped reads (RPKM). Only genes with CPM or a RPKM greater than 1 were retained for differential analysis.

Gene Seat Enrichment Analysis (GSEA)

We used GSEA to determine whether the set of genes upregulated in DDC-treated livers was statistically enriched for genes that were reported to be activated by YAP in Dong et al., 2006 and Yimalamay et al, 2014. GSEA software (http://www.broadinstitute.org/gsea/index.jsp) was applied on RNA-seq expression data preranked by $\log_2$ fold change.

Immunofluorescence

Cells were fixed 10 min at room temperature (RT) with PFA 4%. Slides were permeabilized 10 min at RT with PBS 0.3% Triton X-100, and processed for immunofluorescence according to the following conditions: blocking in Goat Serum (GS, 10%) in PBST for 1.5 hr, followed by incubation with primary antibodies (diluted in 2% GS in PBST) for 16 hr at 4°C, four washes in PBST and incubation with secondary antibodies (diluted in 2% GS in PBST) for 1.5 hr at room temperature. After three washes in PBS, nuclei were stained with ProLong DAPI (Life Technologies).

PFA-fixed paraffin embedded tissue slices were cutted in 10 µm-thick sections. Sections were re-hydrated and antigen retrieval was performed by incubation in citrate buffer 0.01 M pH 6 at 95°C for 20 minutes. Slides were then permeabilized (10 min at RT with PBS 0.3% Triton) and processed as described before.

For immunofluorescence on mammary colonies and organoids, outgrowths freshly recovered from Matrigel were embedded in OCT tissue-freezing medium (PolyFreeze, Sigma) and frozen on dry ice. 8 µm cryostat sections for all types of organoids were cut at –20 °C. Sections were mounted on glass slides and dried for at least 30 min. The sections were then fixed with 4% formaldehyde for 10 min. After washing with PBS the sections were permeabilized 10 min at RT with PBS 0.3% Triton X-100, and processed for immunofluorescence using the following conditions: blocking in 10% Goat Serum (GS) in PBS 0.1% Triton X-100 (PBST) for 1 hr followed by incubation with primary antibodies (diluted in 2% GS in PBST) overnight at 4°C, four washes in PBST and incubation with secondary antibodies (1:200 in 2% GS in PBST) for 2 hours at room temperature. Samples were counterstained with ProLong-DAPI (Molecular Probes, Life Technologies) to label cell nuclei. in PBST for 15 minutes, incubated 20 min with DAPI solution and mounted in glycerol.

Confocal images were obtained with a Leica TCS SP5 equipped with a CCD camera.

Primary antibodies: anti-YAP/TAZ (sc-101199, Santa Cruz), anti-GFP (ab13970; Abcam; efficient to reveal YFP), anti-cytokeratin (wide spectrum screening, ZO622; Dako), anti-cytokeratin 19 (rat anti-*Troma-III* antibody from DSHB), anti-Ki67 (clone SP6; M3062; Spring Bioscience).

anti-a-SMA (A2547; 1:400) mouse monoclonal antibody was from Sigma-Aldrich. anti-K14 (Ab7800; 1:100) mouse monoclonal antibody, anti-K8 (Ab14053; 1:100) chicken polyclonal antibody were from Abcam. anti-p63 (H137, sc-8343; 1:50) polyclonal antibody was from Santa Cruz. *K19* was detected using the monoclonal rat anti-*Troma-III* antibody (DSHB; 1:50). Alexa-conjugated secondary antibodies (Life Technologies): Alexa-Fluor-488 donkey anti-mouse IgG (A21202), Alexa Fluor-488 donkey anti-rabbit IgG (A21206); Alexa Fluor-555 goat anti-chicken IgG (A21437). Goat anti-rat Cy3 (112-165-167) was from Jackson Immunoresearch.

Immunohistochemical stainings were performed on formalin-fixed, paraffin-embedded tissue sections as described in (Cordenonsi et al., 2011). For immunohistochemistry: anti-Ki67 polyclonal antibody (clone SP6; M3062) was from Spring Bioscience; anti-TAZ (anti-WWTR1, HPA007415) was from Sigma; anti-YAP (13584-I-AP) was from Proteintech.

Lentivirus preparation

Lentiviral particles were prepared by transiently transfecting HEK293T (as in Cordenonsi et al., 2011) with lentiviral vectors (10 ug/60 cm ^{2} dishes) together with packaging vectors pMD2-VSVG (2.5 ug) and pPAX2 (7.5 ug) by using TransIT-LT1 (Mirus Bio) according to manufacturer instructions.

Luciferase Assays

Luciferase assays were performed in HEK293 cells with the established YAP/TAZ-responsive luciferase reporter 8xGTIIC-Lux (Dupont et al., 2011). 8xGTIIC-Lux

reporter (50 ng/cm^2) was transfected together with CMV-β-gal (75 ng/cm^2) to normalize for transfection efficiency with CPRG (Roche) colorimetic assay. DNA transfections were done with TransitLT1 (Mirus Bio) according to manufacturer instructions. DNA content in all samples was kept uniform by adding pBluescript plasmid up to 250 ng/cm^2. In experiments in siRNA-depleted cells, cells were first transfected with the indicated siRNAs and, the day after, washed from transfection media, transfected with plasmid DNA, and harvested 48 hr later. Each sample was transfected in duplicate and each experiment was repeated at least three times independently.

Mice

Transgenic lines used in the experiments were gently provided by: Duojia Pan (Zhang et al., 2010) (*Nf2*$^{fl/fl}$); Zhong Wang (*Arid1a*$^{fl/fl}$: these mice have *loxP* sites flanking exon 8) (Gao et al., 2008); Pierre Chambon (*Albumin-CreERT2*)(Stewart et al., 2003); *Taz*$^{fl/fl}$ and double *Yap*$^{fl/fl}$*; Taz*$^{fl/fl}$ conditional knock-out mice were as described in (Azzolin et al., 2014).

Animals were genotyped with standard procedures and with the recommended set of primers (Table 7). Animal experiments were performed adhering to our institutional and national guidelines as approved by OPBA (Padova) and the Ministery of Health of Italy.

Yap, *Taz*, *Arid1a* and *Nf2* conditional knockouts were intercrossed with *Albumin-CreERT2* to obtain the different genotypes used for the experiments. These animals were mixed strains. For the induction of the recombination in the liver, control mice and mice of the indicated genotypes received 1 intraperitoneal injection per *day* of 3 mg Tamoxifen (Sigma) dissolved in corn oil (Sigma) during *5* consecutive days. For the experiments depicted in Figure 3 and 4, mice were kept for 4 months after tamoxifen treatment and then sacrified. For the DDC experiments, after 2 weeks from

tamoxifen treatment, mice were fed with a diet (Mucedola) containing 0.1% DDC (Sigma) for 6 weeks (time point: DDC diet; Figure 5a) and with a normal diet regimen for additional 6 weeks.

Primary mammary epithelial cells (MECs) isolation and induction of yMaSCs

Primary MECs were isolated from the mammary glands of 8- to 12-week-old virgin C57BL/6J mice (unless otherwise specified), according to standard procedures (Stingl et al., 2006). Mammary glands were minced and then digested with 6000 U/ml collagenase I and 2000 U/ml hyaluronidase in the DMEM/F12 at 37°C for 1 hour with vigorous shaking. The digested samples were pipetted, spun down at 1500 rpm for 5 min, and incubated 3 min in 0.64% buffered NH_4Cl in order to eliminate contaminating red blood cells. After washing with DMEM/F12 + 5% FBS, cells were plated for 1 hour at 37°C in DMEM/F12+5% FBS: in this way, the majority of fibroblasts attached to the tissue culture plastic, whereas mammary epithelial populations did not; MEC were thus recovered in the supernatant and pelleted. After washing in PBS/EDTA 0.02%, MECs were further digested with 0.25% trypsin for 5 min and 5 mg/ml dispase plus 100 mg/ml DNase I for other 10 min. The digested cells were diluted in DMEM/F12+5%FBS and filtered through 40 mm cell strainers to obtain single cell suspensions cells and washed once in the same medium.

For separating various MEC subpopulations cells were stained for 30 min at 4°C with antibodies against CD49f (PE-Cy5, cat. 551129, BD Biosciences), CD29 (PE-Cy7, cat. 102222, BioLegend), CD61 (PE, cat. 553347, BD Biosciences), EpCAM (FITC, cat. 118208, BioLegend) and lineage markers (APC mouse Lineage Antibody Cocktail, cat. 51-9003632, BD Biosciences) in DMEM/F12.

The stained cells were then resuspended in PBS/BSA 0,1% and sorted on a BD FACS Aria sorter (BD Biosciences) into luminal differentiated (LD) cells, luminal progenitor (LP) cells and mammary stem cells (MaSCs).

Primary sorted subpopulations from FACS were plated on collagen I-coated supports and cultured in 2D in mammary (MG) medium (DMEM/F12 supplemented with glutamine, antibiotics, murine EGF, murine bFGF, and heparin with 2% FBS).
For induction of yMaSCs, LD cells were transduced for 48 hours with FUW-tetO-YAP, in combination with rtTA-encoding lentiviruses. As a (negative) control, LD cells were transduced with either FUW-tetO-EGFP in combination with rtTA-encoding lentiviruses. After infection, adherent cells were washed and treated with doxycycline for 7 days in MG medium for activating tetracycline-inducible gene expression to obtain "yMaSCs". After doxycycline treatment for 7 days in 2D culture, yMaSCs were processed for further assays or analysis. Unless otherwise specificed, yMaSCs were generated from wild-type YAP (FUW-tetO-wtYAP).

Matrigel culture of mammary colonies and organoids

After infection in 2D cultures and induction with doxycycline for 7 days, mammary cells were detached with trypsin and seeded at a density of 1,000 cells/well in 24-well ultralow attachment plates (Corning) in mammary colony medium (DMEM/F12 containing glutamine, antibiotics, 5% Matrigel, 5% FBS, murine EGF, murine bFGF, and heparin) containing doxycycline (2 mg/ml). Primary colonies were counted 14 days after seeding. To show the self-renewal capacity of yMaSCs independently of exogenous YAP/TAZ supply (i.e, independently of doxycycline administration), primary colonies were recovered from the MG-colony medium by collecting the samples and incubation with an excess volume of ice cold HBSS in order to solubilize Matrigel. After 1 hour, colonies were rinsed 3 times in cold HBSS by centrifugation at 1000 rpm for 5 min and incubated in trypsin 0.05% for 30 min to obtain a single cell suspension. Cells were counted and re-seeded at 1,000 cells/well in 24-well ultralow attachment plates in MG colony medium without doxycycline for further passaging.

For mammary organoid formation, primary colonies were recovered from MG colony medium in cold HBSS and transferred in 100% Matrigel. After Matrigel formed a gel at 37°C, MG organoid medium was added (Advanced DMEM/F12 supplemented with Hepes, GlutaMax, antibiotics, B27, murine EGF, murine bFGF, heparin, Noggin and R-Spondin1). 2 weeks after seeding, organoids were removed from Matrigel, trypsin-dissociated and transferred to fresh Matrigel. Passages were performed in a 1:4-1:8 split ratio every 2 weeks. For analysis, colonies and organoids were recovered from Matrigel as before, and either embedded in OCT medium (PolyFreeze, Sigma) to obtain frozen sections for immunofluorescence or processed for protein or RNA extraction.

Culture of liver organoids

Liver biopsies from mouse and human were harvested in HBSS + P/S 2X and kept cold. Biopsies were washed twice in HBSS + P/S 2X and then manually minced with surgical blade. After this, liver cells were isolated enzymatically with Collagenase type I (Roche): 2000 U/ml for at least 40 minutes at 37°C for mouse and healthy human, soft tissue, and 400U/mL overnight at 37° for tumor human, stiff tissue. The digestion was stopped by dilution adding cold HBSS, the samples were spun down and the supernatant was discarded. The pellet was re-suspended in 1ml of cold emolisi solution and incubated for 3 minutes in ice. The reaction was stopped diluting in HBSS, the sample was spun down, re-suspended in 100 % Matrigel and plated in low attachments plates. After Matrigel formed a gel, Human or Mouse Liver Expansion Medium were added (Huch et al., 2013, see Table 3).

For passaging, organoids embedded in Matrigel were harvested in abundant cold HBSS, pipetted well and spun down. Then they were re-suspended in 10 ml of cold HBSS and kept on ice for 1 hour to facilitate Matrigel melting. After this, the organoids were pelleted down and enzymatically digest with trypsin 0.005% for 10 minutes at

37°C in order to obtain single cells. The reaction was stopped diluting trypsin in HBSS, the cells were spun down, re-suspended in 100% Matrigel and plated as before.

Subcutaneous injections of liver organoids

Both healthy and tumor organoids were expanded and harvested in HBSS + P/S 2X and kept on ice for one hour to let the old matrigel melt. Then, organoids were re-suspended in 100% Matrigel. The injections were performed subcutaneously in NOD/SCID mice.

Matrigel culture of human mammary tumor organoids

Biopsies were minced and then digested with 6000 U/ml collagenase I (Life Technologies) and 2000 U/ml hyaluronidase (Sigma) in the DMEM/F12 (Life Technologies) at 37°C for 3 hours with vigorous shaking. The digested samples were spun down, washed, re-suspended in 100% Matrigel and plated in ultralow attachment plates. After Matrigel solidification, were added the media listed in Figure 8a to the different samples.

For organoids passaging, samples were harvested from Matrigel, washed in cold HBSS and kept on ice for 1 hour in order to allow Matrigel melting. After a series of washing, the samples were either fragmented by mechanical pipetting or digested with trypsin for 20 minutes (with intermediate pipetting) to obtain single cells. In both conditions, cells were re-seeded in 100% Matrigel and plated as above.

FIGURES

FIGURE 1

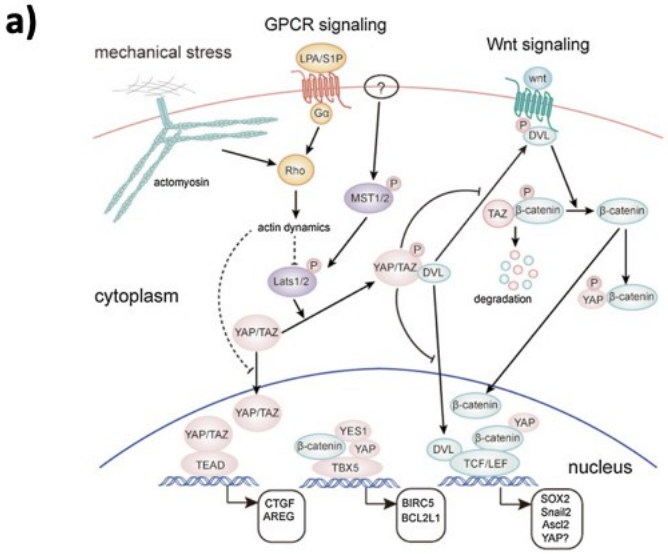
a)
GPCR signaling
mechanical stress
LPA/S1P
Gα
Rho
actomyosin
actin dynamics
MST1/2
P
Lats1/2
cytoplasm
YAP/TAZ
Wnt signaling
wnt
DVL
TAZ
β-catenin
degradation
YAP
nucleus
TEAD
YES1
TBX5
TCF/LEF
CTGF
AREG
BIRC5
BCL2L1
SOX2
Snail2
Ascl2
YAP?

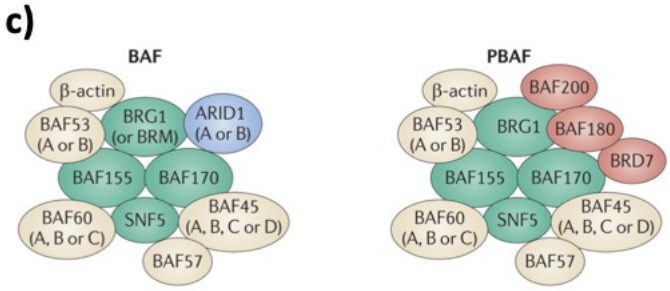
c)
BAF
β-actin
BRG1
(or BRM)
ARID1
(A or B)
BAF53
(A or B)
BAF155
BAF170
BAF60
(A, B or C)
SNF5
BAF45
(A, B, C or D)
BAF57
PBAF
β-actin
BAF200
BAF53
(A or B)
BRG1
BAF180
BRD7
BAF155
BAF170
BAF60
(A, B or C)
SNF5
BAF45
(A, B, C or D)
BAF57

FIGURE 1

a) A schematic representation of some of the possible regulators of the YAP/TAZ signaling pathway.

b) Schematic representation of SWI/SNF complexes.

FIGURE 2

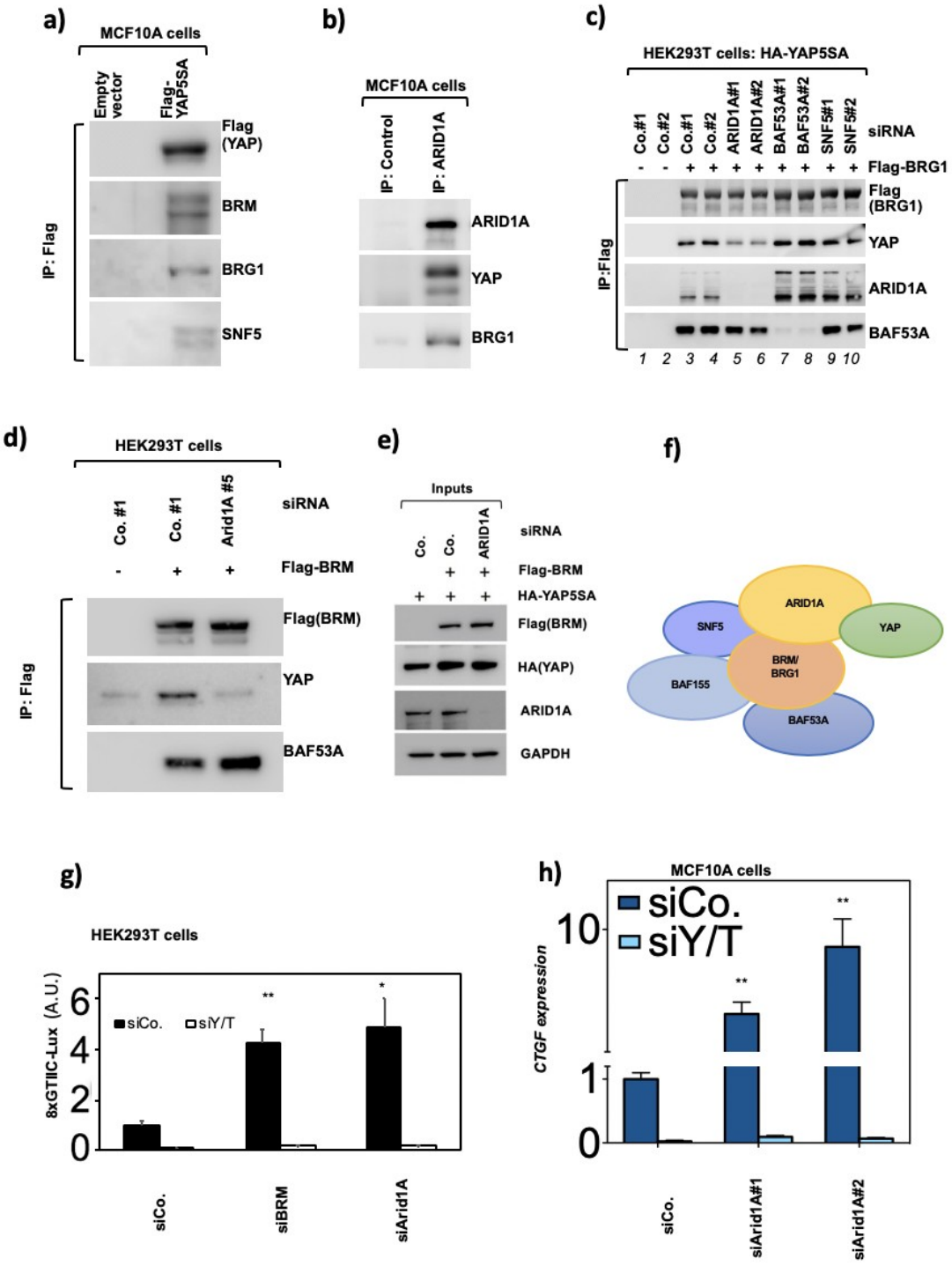
a)
MCF10A cells
Empty vector
Flag-YAP5SA
IP: Flag
Flag (YAP)
BRM
BRG1
SNF5
b)
MCF10A cells
IP: Control
IP: ARID1A
ARID1A
YAP
BRG1
c)
HEK293T cells: HA-YAP5SA
siRNA
Co.#1
Co.#2
Co.#1
Co.#2
ARID1A#1
ARID1A#2
BAF53A#1
BAF53A#2
SNF5#1
SNF5#2
Flag-BRG1
IP:Flag
Flag (BRG1)
YAP
ARID1A
BAF53A
1 2 3 4 5 6 7 8 9 10
d)
HEK293T cells
siRNA
Co. #1
Co. #1
Arid1A #5
Flag-BRM
IP: Flag
Flag(BRM)
YAP
BAF53A
e)
Inputs
siRNA
Co.
Co.
ARID1A
Flag-BRM
HA-YAP5SA
Flag(BRM)
HA(YAP)
ARID1A
GAPDH
f)
ARID1A
SNF5
YAP
BRM/ BRG1
BAF155
BAF53A
g)
HEK293T cells
8xGTIIC-Lux (A.U.)
siCo.
siY/T
siCo.
siBRM
siArid1A
h)
MCF10A cells
siCo.
siY/T
CTGF expression
siCo.
siArid1A#1
siArid1A#2

FIGURE 2

a) Western blot visualizing proteins co-precipitated with YAP in MCF10A stably transduced with Flag-YAP 5SA or with the corresponding empty vector, after anti-Flag immunoprecipitation.

b) Western blot showing ARID1a co-precipitating proteins in lysates of MCF10A cells subjected to anti-ARID1a immunoprecipitation.

c) Western blot showing, in HEK293T extracts, proteins co-precipitated with BRG1. Cells were transfected with independent siRNA for indicated genes (ARID1a in lanes 5 and 6; BAF53a in lanes 7 and 8; SNF5 in lanes 9 and 10) and siRNA control (in lanes 1, 2, 3 and 4) and with plasmid encoding Flag-BRG1 as indicated. Cell lysates were subjected to anti-Flag immunoprecipitation.

d) Western blot showing, in HEK293T extracts, proteins co-precipitated with BRM. Cells were transfected with siRNA for ARID1a, siRNA control and with plasmid encoding Flag-BRM as indicated. Cell lysates were subjected to anti-Flag immunoprecipitation.

e) Western blots of the inputs of the immunoprecipitation experiment shown in Figure 2b. HEK293T cells were transfected with control (Co.) siRNA or siRNA against *ARID1A* and with plasmids encoding HA–YAP(5SA) and Flag–BRM, as indicated.

f) Schematic representation of the interaction between YAP/TAZ and the SWI/SNF complex.

g) Luciferase assay performed in HEK293T cells with 8xGTIIC-Lux reporter to trace YAP/TAZ-dependent transcriptional activity. Cells were transfected with indicated siRNAs to deplete the endogenous genes. Data are mean + s.d. of $n = 3$ biologically independent samples; *P* values were determined by unpaired two-sided Student's *t*-test. Representative experiments are shown, which were repeated independently or three times, all with similar results (* means $P \leq 0.05$; ** means $P \leq 0.01$).

h) qRT-PCR for CTGF expression levels in MCF10a cells transfected with independent siRNAs against ARID1a and with control siRNA, both in combination with siRNA against YAP/TAZ. Data are mean + s.d. of $n = 3$ biologically independent samples; *P* values were determined by unpaired two-sided Student's *t*-

test. Representative experiments are shown, which were repeated independently or three times, all with similar results (* means $P \leq 0.05$; ** means $P \leq 0.01$).

FIGURE 3

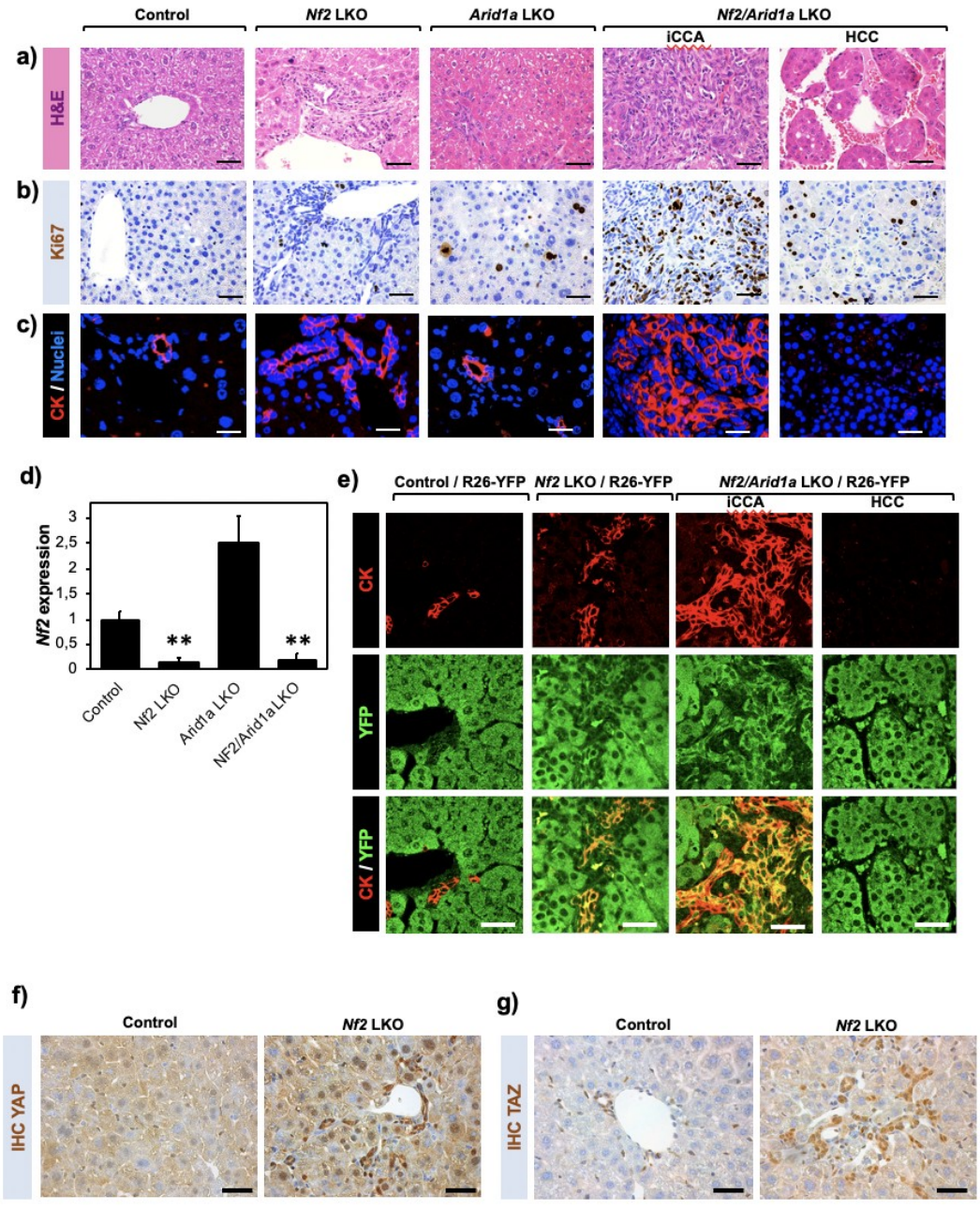
Control
Nf2 LKO
Arid1a LKO
Nf2/Arid1a LKO
iCCA
HCC
a)
H&E
b)
Ki67
c)
CK / Nuclei
d)
Nf2 expression
3
2,5
2
1,5
1
0,5
0
**
**
Control
Nf2 LKO
Arid1a LKO
NF2/Arid1aLKO
e)
Control / R26-YFP
Nf2 LKO / R26-YFP
Nf2/Arid1a LKO / R26-YFP
iCCA
HCC
CK
YFP
CK / YFP
f)
Control
Nf2 LKO
IHC YAP
g)
Control
Nf2 LKO
IHC TAZ

FIGURE 3

a) H&E (scale bars, 100µm), **b)** Ki67 (scale bars, 100µm) and **c)** CK (scale bars, 100µm) stainings in liver sections from control mice (*n* = 6 mice), and *Nf2* (*n* = 6 mice), *Arid1a* (*n* = 7 mice) and *Nf2/Arid1a* (*n* = 7 mice) liver knockout (LKO) mutant mice, four months after tamoxifen treatment. The knockout of Nf2 or Arid1a alone had only minimal effects. The double Nf2/Arid KO mice displayed cholangiocarcinoma and hepatocellular carcinoma.

d) qRT-PCR analysis for *Nf2* expression in the livers of control (*n* = 6 mice), and *Nf2* (*n* = 6 mice), *Arid1a* (*n* = 7 mice) and *Nf2/Arid1a* (*n* = 7 mice) liver mutant (LKO) mice, four months after tamoxifen treatment, normalized to *Gapdh*. All animals were included. Mean and data for individual mice are shown.

e)YFP and CK staining in liver sections of *R26-YFP* ctrl mice (n = 6), *R26-YFP/Nf2* KO mice (n = 6) and *R26-YFP/Nf2/Arid1a* KO mice (n=7). The staining confirmed the hepatocyte specificity of the knockout.

f) Yap and **g)** Taz immunohistochemistry in liver sections of control and *Nf2* knockout mice. Representative images of experiments that were independently replicated using three mice for each genotype, with similar results

FIGURE 4

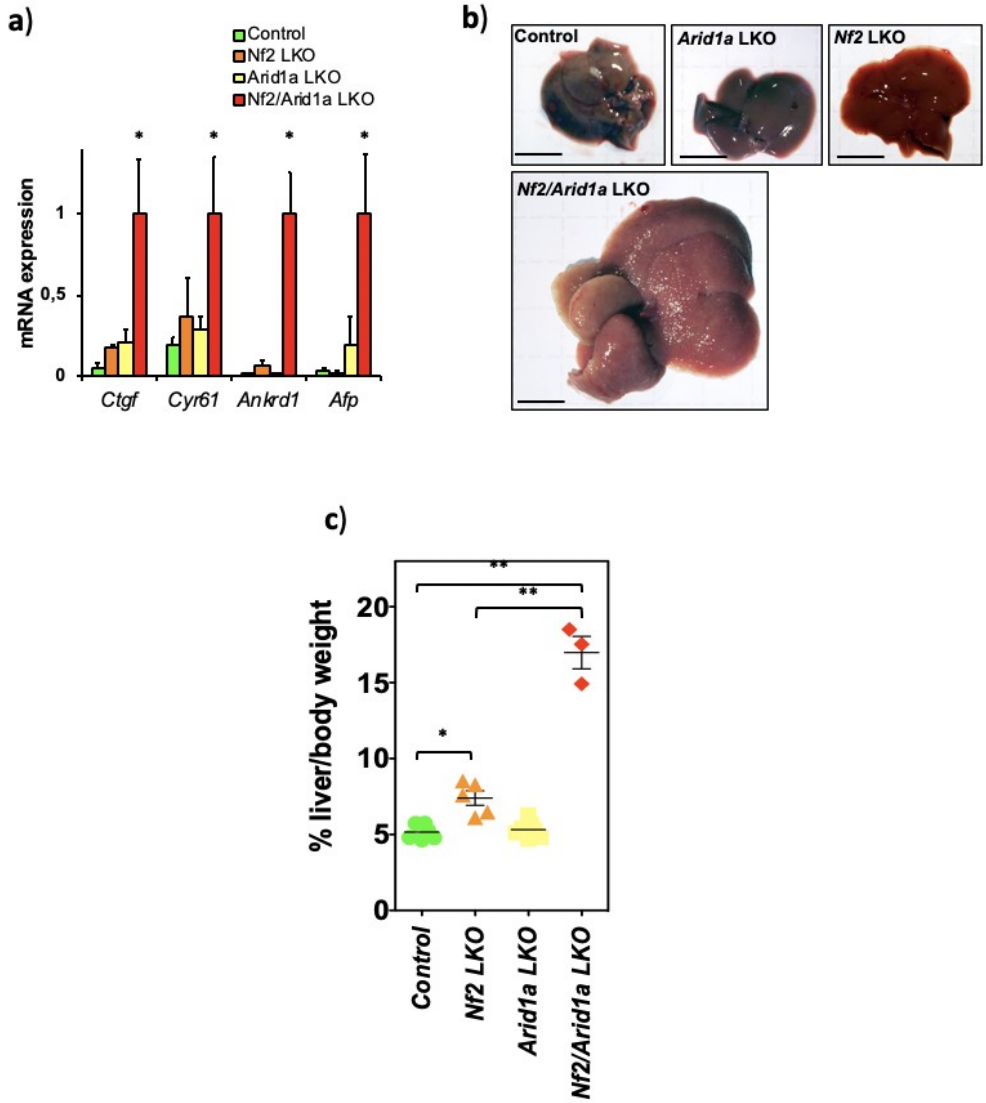
a)
Control
Nf2 LKO
Arid1a LKO
Nf2/Arid1a LKO
mRNA expression
1
0,5
0
Ctgf
Cyr61
Ankrd1
Afp
b)
Control
Arid1a LKO
Nf2 LKO
Nf2/Arid1a LKO
c)
% liver/body weight
20
15
10
5
0
Control
Nf2 LKO
Arid1a LKO
Nf2/Arid1a LKO

FIGURE 4

a) qRT-PCR analysis for YAP/TAZ target genes (*Ctgf, Cyr61, Ankrd1*) and *Afp* expression in the livers of the indicated genotypes, normalized to *Gapdh* expression. The double *Nf2/Arid1a* KO induces massive upregulations of the investigated genes. All animals were included. Data are normalized to *Nf2/Arid1a* LKO mice. Data are mean + s.d. for same number of mice per genotype as in Figure 1d.

b) Gross liver images from control mice ($n = 6$ mice), and *Nf2* ($n = 6$ mice), *Arid1a* ($n = 7$ mice) and *Nf2/Arid1a* ($n = 7$ mice) liver knockout (LKO) mutant mice four months after tamoxifen treatment (scale bars, 1 cm).

c) Liver-to-body weight ratio from control mice ($n = 6$ mice), *Nf2* ($n = 6$ mice), *Arid1a* ($n = 7$ mice) and *Nf2/Arid1a* ($n = 7$ mice) LKO mutant mice, four months after tamoxifen treatment. *P* values were determined by one-way analysis of variance (ANOVA) with Tukey's multiple comparisons test.

FIGURE 5

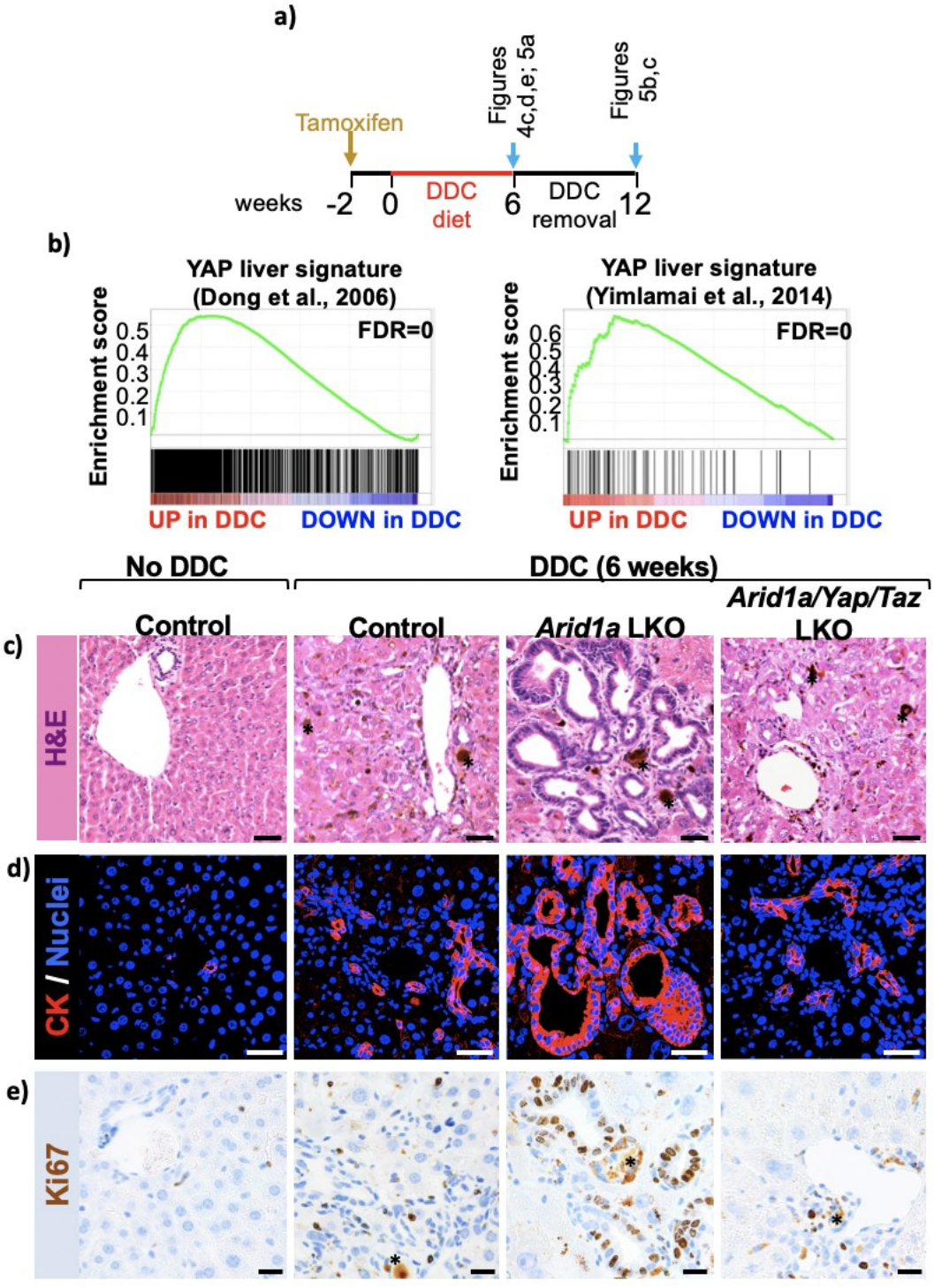
a)
Tamoxifen
Figures 4c,d,e; 5a
Figures 5b,c
weeks -2 0 DDC diet 6 DDC removal 12
b)
YAP liver signature (Dong et al., 2006)
FDR=0
Enrichment score
0.5
0.4
0.3
0.2
0.1
UP in DDC
DOWN in DDC
YAP liver signature (Yimlamai et al., 2014)
FDR=0
Enrichment score
0.6
0.5
0.4
0.3
0.2
0.1
UP in DDC
DOWN in DDC
No DDC
DDC (6 weeks)
Control
Control
Arid1a LKO
Arid1a/Yap/Taz LKO
c)
H&E
d)
CK / Nuclei
e)
Ki67

FIGURE 5

a) Schematic representation of the experiments depicted in figure 4 and 5. DDC diet was administrated to mice diet for 6 weeks, then a normal diet was administrated for additional 6 weeks.

b) GSEA analysis of genes differentially expressed between control and DDC-fed (6 weeks) mouse livers using two different liver-specific YAP gene signatures (Dong et al., 2007; Yimlamai et al., 2014).

c) H&E (scale bars, 40μm), **d)** CK (scale bars, 40μm) and **e)** Ki67 (scale bars, 20μm) stainings of liver sections from control (n = 10), *Arid1a* LKO (n = 12), and *Arid1a/Yap/Taz* LKO (n = 15) mice treated with tamoxifen and then fed a DDC diet, compared to control mice fed a normal diet (n = 10). Cholangiocarcinomatous lesions can be noticed in *Arid1a* KO mice liver sections (CK-positive, Ki67-positive), while they are completely absent in *Arid1a/Yap/Taz* KO mice. Asterisks (*) indicate porfirin deposits, typically present in liver of animals treated with DDC.

FIGURE 6

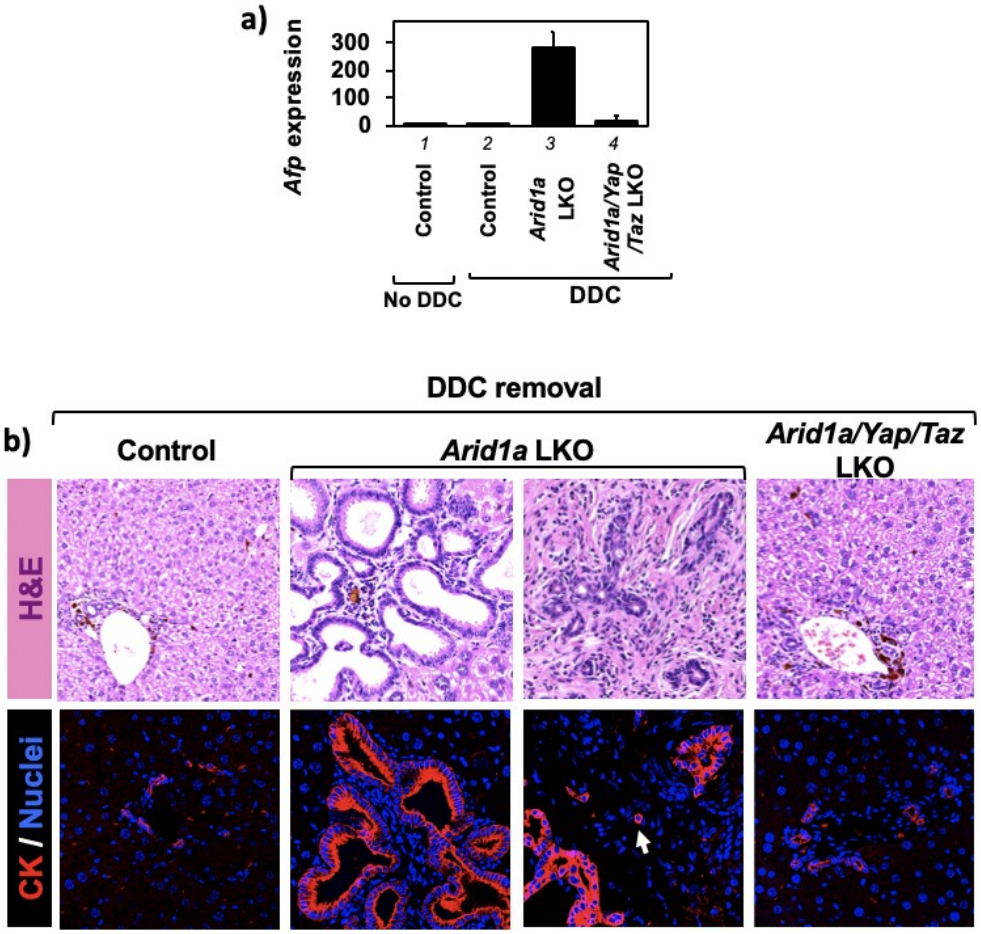
a)
Afp expression
300
200
100
0
1
2
3
4
Control
Control
Arid1a LKO
Arid1a/Yap /Taz LKO
No DDC
DDC
DDC removal
b)
Control
Arid1a LKO
Arid1a/Yap/Taz LKO
H&E
CK / Nuclei

FIGURE 6

a) qRT-PCR analysis for *Afp* expression in the livers of control (n = 4), *Arid1a* LKO (n = 5), *Arid1a/Yap/Taz* LKO (n = 5) mice treated with tamoxifen and then DDC, normalized to Gapdh expression. The double *Arid1a/Yap/Taz* KO rescued the upregulations of *Afp* obtained in *Arid1a* KO under DDC treatment. Data are normalized to livers of mice not treated with DDC (n = 4). Data are mean + s.d. of the indicated number of mice. This experiment was independently repeated three times with similar results, analysing, in total, at least 10 mice for each genotype.
b) H&E (top; scale bars, 75 μm) and cytokeratin (bottom; scale bars,48μm) stainings of liver sections from the indicated mice 6 weeks after DDC removal. Cholangiocarcinomatous lesions with dysplastic glandular structures persisted in the *Arid1a* KO mice even after DDC removal; in contrast, such lesions were never observed in control or *Arid1a/Yap/Taz* KO mice.

FIGURE 7

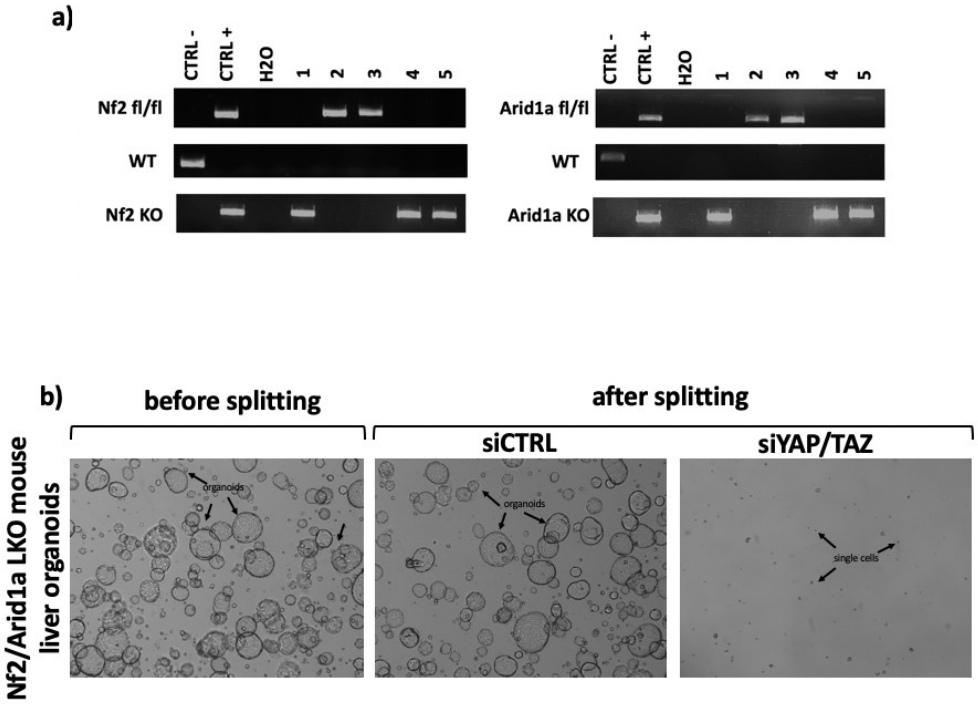
a)
CTRL -
CTRL +
H2O
1
2
3
4
5
Nf2 fl/fl
WT
Nf2 KO
Arid1a fl/fl
WT
Arid1a KO
b)
before splitting
after splitting
siCTRL
siYAP/TAZ
Nf2/Arid1a LKO mouse liver organoids
organoids
organoids
single cells

FIGURE 7

a) Genomic DNA was extracted from clonal culture of organoids obtained from liver of mice bearing liver-specific knockout of Nf2 and Arid1a alleles to verify tamoxifen-induced recombination and select only the recombined clones. Panels are PCR bands for the indicated recombined alleles.

b) Representative pictures of organoids obtained by *Nf2/Arid1a* KO liver, transfected with siRNA CTRL or siRNA for YAP/TAZ after dissociation at single cells level. Only organoids transfected with siCTRL were able to regrow after seeding. Magnification is the same for all pictures.

FIGURE 8

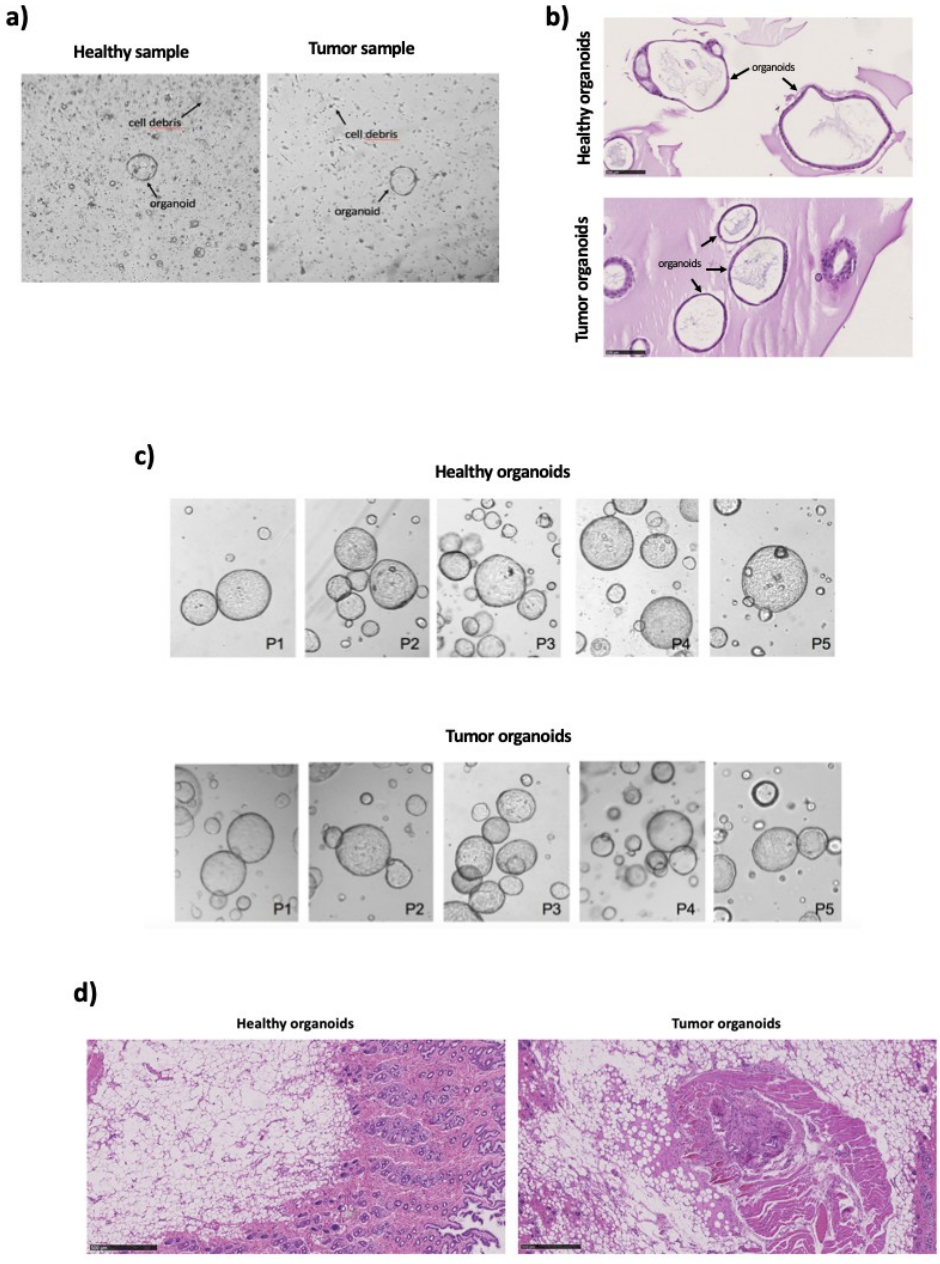
a)
Healthy sample
Tumor sample
cell debris
organoid
cell debris
organoid
b)
Healthy organoids
organoids
Tumor organoids
organoids
c)
Healthy organoids
P1
P2
P3
P4
P5
Tumor organoids
P1
P2
P3
P4
P5
d)
Healthy organoids
Tumor organoids

FIGURE 8

a) Representative images of cyst-shaped organoids growing from healthy and cholangiocarcinoma human liver samples. Magnification is the same for all pictures
b) H&E staining of organoids from healthy and cholangiocarcinoma human liver samples (scale bars, 100 μm).
c) Representative images of human healty and tumor organoids passaged trough time. Magnification is the same for all pictures.
d) H&E staining of the small masses found in the sites of subcutaneous injections after injections of human healty and tumor organoid (scale bars, 500 μm).

FIGURE 9

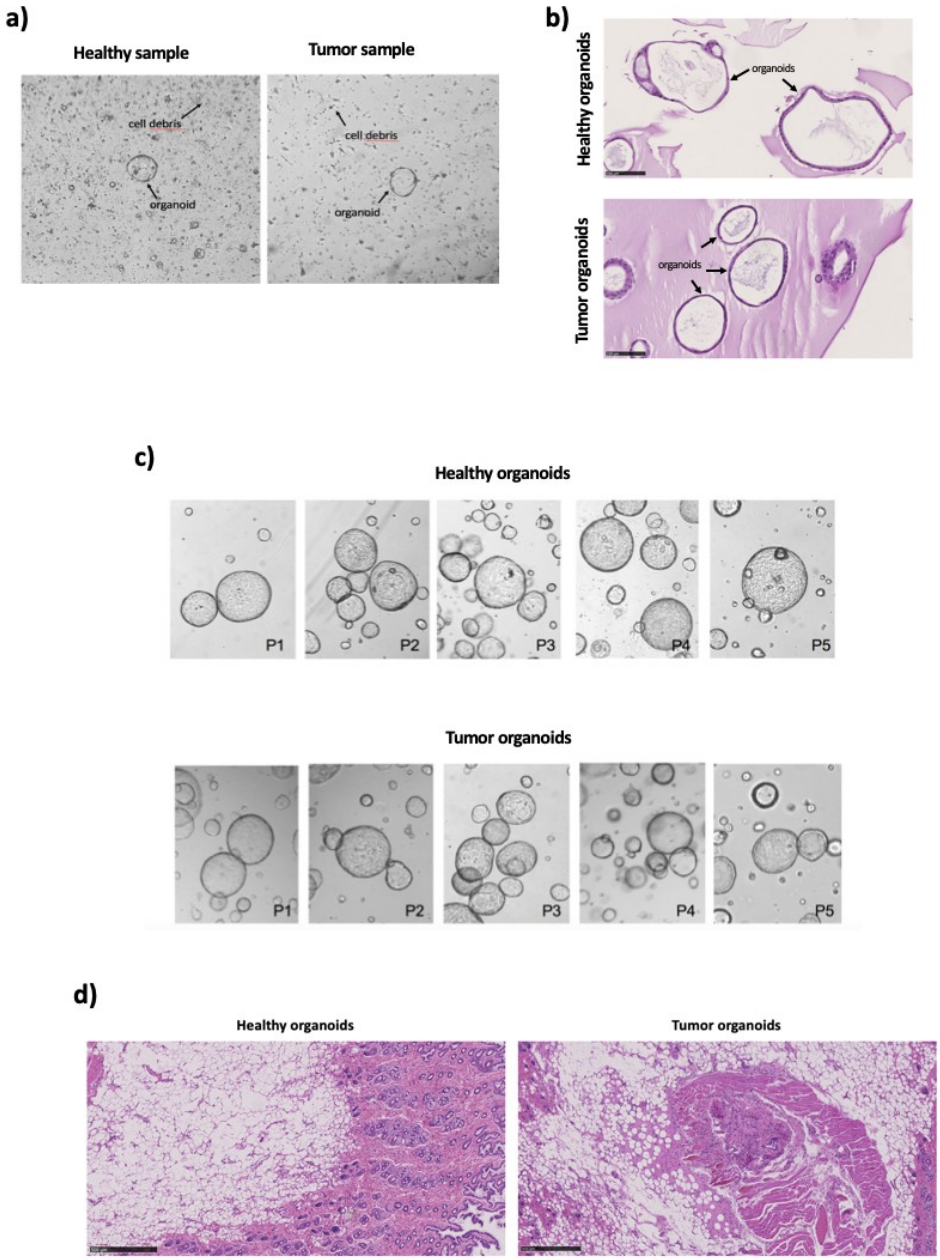
a)
Healthy sample
Tumor sample
cell debris
organoid
cell debris
organoid
b)
Healthy organoids
organoids
Tumor organoids
organoids
c)
Healthy organoids
P1
P2
P3
P4
P5
Tumor organoids
P1
P2
P3
P4
P5
d)
Healthy organoids
Tumor organoids

FIGURE 9

a) Immunostainings for K14/K8 at different timing of the colonies growth and for **b)** alpha-SMA in colonies originating from yMaSCs (scale bars, 36 μm).

c) Quantifications of individual cells inside the colonies that are positive for the previously indicated markers.

d) Heatmap of genes differentially expressed between LD cells, yMaSCs colonies (two independent preparations) and MaSC-enriched cell population (MaSCs).

e) qRT-PCR comparing FACS-purified MaSCs from the mammary gland and yMaSC colonies. Purified LD cells were used as control. Data are normalized to *Gapdh* expression and are referred to LD levels for all the luminal genes, to MaSCs levels for myoepithelial and basal genes, and to yMaSC colonies levels for yMaSC specific genes (each set to 1).

f) Immunofluorescence stainings for K14, K8, alpha-SMA, K19 and p63 in organoids obtained from MaSCs and yMaSCs colonies. (Scale bars, 17 μm),

FIGURE 10

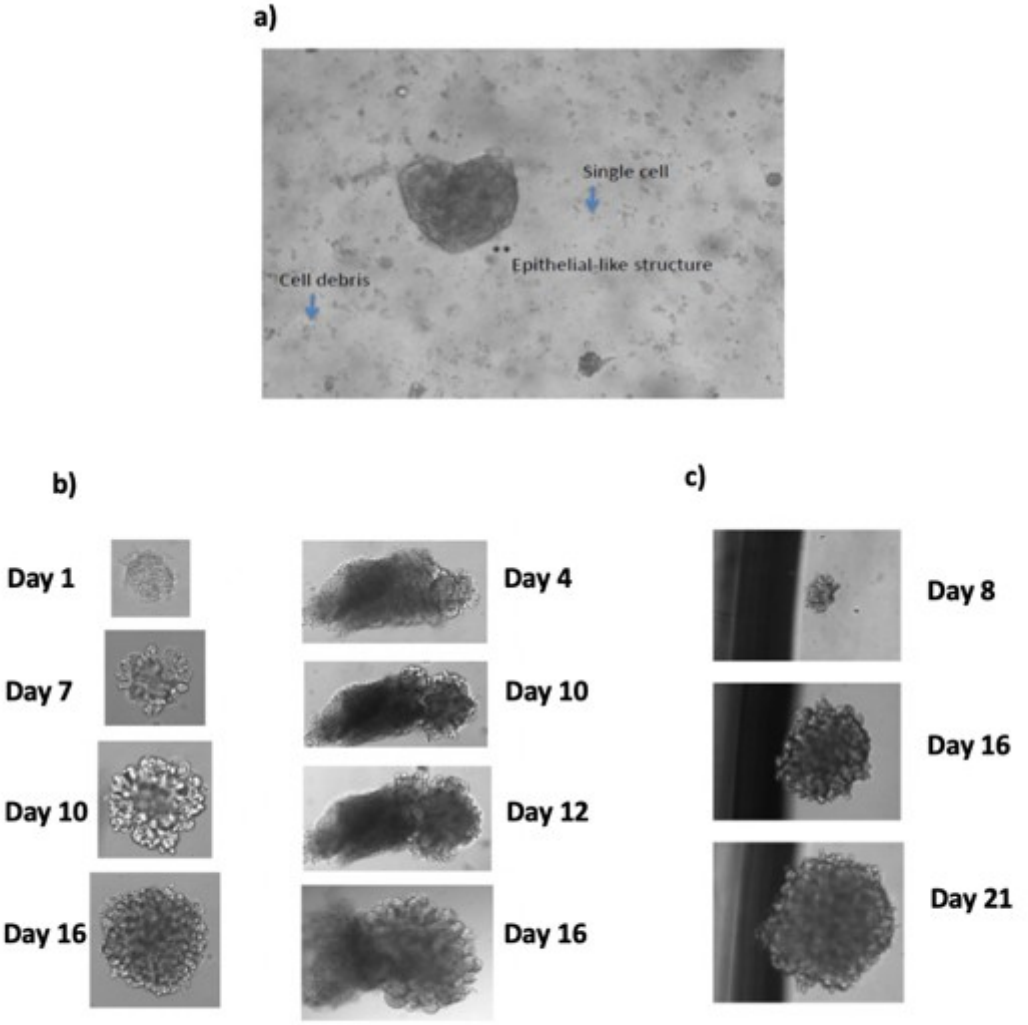
a)
Single cell
Epithelial-like structure
Cell debris
b)
Day 1
Day 7
Day 10
Day 16
Day 4
Day 10
Day 12
Day 16
c)
Day 8
Day 16
Day 21

FIGURE 10

a) Representative image of mammary tumor sample plated after dissociation protocol.

b) Representative images of primary outgrowths development from HMaTuORG_001 and **c)** HMaTuORG_002 trough time.

TABLE 1

Some YAP-interacting proteins identified by MS.

Accession Number	MW	Empty vector	Flag-YAP-5SA
TEAD1_HUMAN	48 kDa	0	6
TEAD2_HUMAN	49 kDa	0	1
TEAD3_HUMAN	49 kDa	0	16
TEAD4_HUMAN	48 kDa	0	4
LATS1_HUMAN	127 kDa	0	17
LATS2_HUMAN	120 kDa	0	6
ZYX_HUMAN	61 kDa	0	2
MPDZ_HUMAN	222 kDa	0	19
PTN14_HUMAN	135 kDa	0	29
WWC2_HUMAN	134 kDa	0	1
WWC3_HUMAN	123 kDa	0	9
CTNA1_HUMAN	100 kDa	1	1
ZO1_HUMAN	195 kDa	0	0
ZO2_HUMAN	134 kDa	0	1
INADL_HUMAN	196 kDa	0	23
LIN7C_HUMAN	22 kDa	0	4
MERL_HUMAN	70 kDa	0	21
MPP5_HUMAN	77 kDa	0	9
AMOL1_HUMAN	107 kDa	0	30
AMOL2_HUMAN	86 kDa	0	44

TABLE 2

Association of YAP with several components of the SWI/SNF chromatin-remodeling complex, identified by MS. The Table shows the number of peptide recognized to interact with YAP. The interaction is significant when 1.

Accession Number	MW	Empty vector	Flag-YAP-5SA
ARID1A_HUMAN	242 kDa	0	4
ARID1B_HUMAN	236 kDa	0	0
BRG1_HUMAN	185 kDa	0	2
SMARCC1_HUMAN	123 kDa	0	1
BAF53a_HUMAN	47 kDa	0	3
SMARCA5_HUMAN	122 kDa	0	1
PARD3_HUMAN	151 kDa	0	0
RPGF6_HUMAN	179 kDa	0	0
EZRI_HUMAN	69 kDa	0	0
UBA1_HUMAN	118 kDa	0	0
CTRO_HUMAN	231 kDa	0	0
CKAP4_HUMAN	66 kDa	0	0
RASF8_HUMAN	48 kDa	0	0
ARHG2_HUMAN	112 kDa	0	0
CAP1_HUMAN	52 kDa	0	1
TPPC9_HUMAN	129 kDa	0	0
IF4G1_HUMAN	175 kDa	0	0
C1TM_HUMAN	106 kDa	0	0
TET2_HUMAN	224 kDa	0	0
E2F7_HUMAN	100 kDa	0	0
EMD_HUMAN	29 kDa	0	0

HMHA1_HUMAN	125 kDa	0	0
HNRL1_HUMAN	96 kDa	0	0
MCM2_HUMAN	102 kDa	0	0
MSH6_HUMAN	153 kDa	0	0
RNC_HUMAN	159 kDa	0	0
STAT1_HUMAN	87 kDa	0	0
XRCC5_HUMAN	83 kDa	0	29
XRCC6_HUMAN	70 kDa	0	34
MYH9_HUMAN	227 kDa	3	22
ANM5_HUMAN	73 kDa	3	12

TABLE 3

Organoids Expansion Medium.

Supplement	**From**	**Concentration**
N2	Gibco	1%
B27	Gibco	1%
NAC	Sigma	1,25 mM
Gastrin	Sigma	10 nM
hEGF	Peprotech	50 ng/mL
hFGF10	Peprotech	100 ng/mL
HGF	Peprotech	25 ng/mL
Nicotinamide	Sigma	10 mM
A83.01	Tocris	5 µM
Forskolin	Sigma	10 µM
hR-SPO1	Sino Biol	1 µg/mL
in Advance DMEM/F12 from Gibco		

TABLE 4

Mammary tumor sample plated after dissociation protocol.

Code	Diagnosi	Dissociation	Culture conditions
HMaTuORG_001	Triple neg	3 h	100 % Matrigel + DMEM/F12 containing glutamine, antibiotics, 5% FBS, EGF, bFGF, and heparin
HMaTuORG_002	HER2+	o.n.	100% Matrigel + 1) EGF/Noggin/R-Spondin (ENR)-based organoid medium; 2) ENR medium + progesterone; 3) ENR + oestrogen; 4) ENR + progesterone + oestrogen
HMaTuORG_003	Triple neg	o.n.	100% Matrigel + 1)ENR medium; 2)ENR medium +NAC; 3)ENR medium +Cholera toxin+ Insulin
HMaTuORG_004	HER2+	o.n.	100% Matrigel + medium containing ROCKi, A-83-01, Noggin, and CHIR99021
HMaTuORG_006	HER2+	o.n.	100% Matrigel + medium containing ROCKi, A-83-01, Noggin, and CHIR99021

TABLE 5

RNAi sequences.

siRNA	**Interfering sequence** (target)
Control#1	AllStars Negative Control siRNA (QIAGEN)
Control#2	TTCTCCGAACGTGTCACGT
human	
ARID1a#1	GGCGGGAACTTGCAACCAA
ARID1a#2	CGGTATCACCGTTGATGAA
BRG1#1	GCGCTACAACCAGATGAAA
BRG1#2	ACTGGATGTCAAACAGTAA
BRM#1	GCGTCTACATAAGGTGTTA
BRM#2	CCGCATAGCTCATAGGATA
YAP#1	GACATCTTCTGGTCAGAGA
YAP#2	CTGGTCAGAGATACTTCTT
TAZ#1	ACGTTGACTTAGGAACTTT
TAZ#2	AGGTACTTCCTCAATCACA
mouse	
Yap	TCTCTGACCAGAAGATGTC
Taz	ACGTTGACTTAGGAACTTT

TABLE 6

List of primers used for qRT-PCR.

Gene	Forward primer	Reverse primer
human		
GAPDH	AGCCACATCGCTCAGACAC	GCCCAATACGACCAAATCC
CTGF	AGGAGTGGGTGTGTGACGA	CCAGGCAGTTGGCTCTAATC
mouse		
Gapdh	ATCCTGCACCACCAACTGCT	GGGCCATCCACAGTCTTCTG
Nf2	ACACTGGGGCTTCGGGAAAC	ATTTTGAGCCAGGCCACCGT
Afp	GATTCCTCCCAGTGCGTGAC	CCCATCGCCAGAGTTTTTCTT
a-Sma	TGCTGTCCCTCTATGCCTCT	GAAGGAATAGCCACGCTCAG
Aldh1L1	CAGGAGGTTTACTGCCAGCTA	CACGTTGAGTTCTGCACCCA
AnkrD1	CTGTGAGGCTGAACCGCTAT	TCTCCTTGAGGCTGTCGAAT
AnkrD1	CTGTGAGGCTGAACCGCTAT	TCTCCTTGAGGCTGTCGAAT
Areg	TGGTGAACGGTGTGGAGAAA	TGTGATAACGATGCCGATGC
K18	ATGACACCAACATCACAAGG	ATCCACTTCCACAGTCAATC
K19	AGGAGCTGAACACCCAGGTC	GGGCTTCAAAACCGCTGAT
K6	ACCACCACCTCCTCCAGCAA	ACACAGCCTCCTCAGTCCCA
Foxa1	ACAGCTACTACGCGGACACG	GCTCGTGGTCATGGTGTTCA
Erbb3	TGCCAGATACGCACCTCAGA	TACCCCTCCTCTTCCGGTTC
K14	AGGACCTGAAGAGCAAGATC	TCCTTGAGGCTCTCAATCTG
K5	TCTCTTCTGGCTACGGAGGA	GAAGCTCATGCCTCCTTGAC
Myh11	GGTGAACGCCCTCAAGAGCA	TCTGAGTCCCGAGCGTCCAT
DNp63	CCTGGAAAACAATGCCCAGAC	GAGGAGCCGTTCTGAATCTGC
Procr	GGAGAAAGGGCTGGACTGGT	CCCCTCCCACACACACACTT

Nestin	CCCTGAAGTCGAGGAGCTG	CTGCTGCACCTCTAAGCGA
Ctgf	CTGCCTACCGACTGGAAGAC	CATTGGTAACTCGGGTGGAG

TABLE 7

List of primers used for genotyping PCR.

Gene	Forward primer	Reverse primer
mouse		
Nf2 fl/fl	CTTCCCAGACAAGCAGGGTTC	GAAGGCAGCTTCCTTAAGTC
Nf2 KO	GAAGGCAGCTTCCTTAAGTC	CTCTATTTGAGTGCGTGCCATG
Arid1a fl/fl	TGTTCATTTTTGTGGCGGGAG	AACCATGGCCAACAATTCAG
Arid1a KO	GTAATGGGAAAGCGACTACTGGAG	TGTTCATTTTTGTGGCGGGAG

REFERENCES

Aragona, M. *et al.* A Mechanical Checkpoint Controls Multicellular Growth through YAP/TAZ Regulation by Actin-Processing Factors. *Cell* **154**, 1047–1059 (2013).

Asselin-Labat, M. L. *et al.* Control of mammary stem cell function by steroid hormone signalling. *Nature* (2010). doi:10.1038/nature09027

Azzolin, L. *et al.* YAP/TAZ incorporation in the β-catenin destruction complex orchestrates the Wnt response. *Cell* (2014). doi:10.1016/j.cell.2014.06.013

Bartucci, M. *et al.* TAZ is required for metastatic activity and chemoresistance of breast cancer stem cells. *Oncogene* (2015). doi:10.1038/onc.2014.5

Benhamouche, S. *et al.* Nf2/Merlin controls progenitor homeostasis and tumorigenesis in the liver. *Genes Dev.* (2010). doi:10.1101/gad.1938710

Biegel, J. A. *et al.* Germ-line and acquired mutations of INI1 in atypical teratoid and rhabdoid tumors. *Cancer Res.* (1999).

Boj, S. F. *et al.* Organoid models of human and mouse ductal pancreatic cancer. *Cell* (2015). doi:10.1016/j.cell.2014.12.021

Brivio, S., Cadamuro, M., Strazzabosco, M. & Fabris, L. Tumor reactive stroma in cholangiocarcinoma: The fuel behind cancer aggressiveness. *World Journal of Hepatology* (2017). doi:10.4254/wjh.v9.i9.455

Bultman, S. *et al.* A Brg1 null mutation in the mouse reveals functional differences among mammalian SWI/SNF complexes. *Mol. Cell* (2000). doi:10.1016/S1097-2765(00)00127-1

Cai, X., Chiu, Y. H. & Chen, Z. J. The cGAS-cGAMP-STING pathway of cytosolic DNA sensing and signaling. *Mol. Cell* **54**, 289–296 (2014).

Camargo, F. D. *et al.* YAP1 Increases Organ Size and Expands Undifferentiated Progenitor Cells. *Curr. Biol.* (2007). doi:10.1016/j.cub.2007.10.039

Caponigro, G. & Sellers, W. R. Advances in the preclinical testing of cancer therapeutic hypotheses. *Nature Reviews Drug Discovery* (2011). doi:10.1038/nrd3385

Chang, L. *et al.* The SWI/SNF complex is a mechanoregulated inhibitor of YAP and TAZ. *Nature* (2018). doi:10.1038/s41586-018-0658-1

Chen, Q. *et al.* A temporal requirement for Hippo signaling in mammary gland differentiation, growth, and tumorigenesis. *Genes Dev.* (2014). doi:10.1101/gad.233676.113

Cirri, P. & Chiarugi, P. Cancer associated fibroblasts: the dark side of the coin. *Am. J. Cancer Res.* (2011).

Clevers, H. Wnt/β-Catenin Signaling in Development and Disease. *Cell* (2006). doi:10.1016/j.cell.2006.10.018

Clevers, H. & Tuveson, D. A. Organoid Models for Cancer Research. *Annu. Rev. Cancer Biol.* (2019). doi:10.1146/annurev-cancerbio-030518-055702

Cordenonsi, M. *et al.* The hippo transducer TAZ confers cancer stem cell-related traits on breast cancer cells. *Cell* (2011). doi:10.1016/j.cell.2011.09.048

De La Serna, I. L., Ohkawa, Y. & Imbalzano, A. N. Chromatin remodelling in mammalian differentiation: Lessons from ATP-dependent remodellers. *Nature Reviews Genetics* (2006). doi:10.1038/nrg1882

Diehn, M. *et al.* Association of reactive oxygen species levels and radioresistance in cancer stem cells. *Nature* (2009). doi:10.1038/nature07733

Dong, J. *et al.* Elucidation of a Universal Size-Control Mechanism in Drosophila and Mammals. *Cell* (2007). doi:10.1016/j.cell.2007.07.019

Drost, J. & Clevers, H. Organoids in cancer research. *Nature Reviews Cancer* (2018). doi:10.1038/s41568-018-0007-6

Dupont, S. *et al.* Role of YAP/TAZ in mechanotransduction. *Nature* (2011). doi:10.1038/nature10137

Dykhuizen, E. C. *et al.* BAF complexes facilitate decatenation of DNA by topoisomerase IIα. *Nature* (2013). doi:10.1038/nature12146

Enzo, E. *et al.* Aerobic glycolysis tunes YAP / TAZ transcriptional activity . *EMBO J.* (2015). doi:10.15252/embj.201490379

Feng, J. *et al.* Verteporfin, a suppressor of YAP–TEAD complex, presents promising antitumor properties on ovarian cancer. *Onco. Targets. Ther.* (2016). doi:10.2147/OTT.S109979

Flowers, S., Nagl, N. G., Beck, G. R. & Moran, E. Antagonistic roles for BRM and BRG1 SWI/SNF complexes in differentiation. *J. Biol. Chem.* (2009). doi:10.1074/jbc.M808782200

Fujii, M. *et al.* A Colorectal Tumor Organoid Library Demonstrates Progressive Loss of Niche Factor Requirements during Tumorigenesis. *Cell Stem Cell* (2016). doi:10.1016/j.stem.2016.04.003

Fumagalli, A. *et al.* Genetic dissection of colorectal cancer progression by orthotopic transplantation of engineered cancer organoids. *Proc. Natl. Acad. Sci. U. S. A.* (2017). doi:10.1073/pnas.1701219114

Gao, D. *et al.* Endothelial progenitor cells control the angiogenic switch in mouse lung metastasis. *Science (80-.).* (2008). doi:10.1126/science.1150224

Gao, D. *et al.* Organoid cultures derived from patients with advanced prostate cancer. *Cell* (2014). doi:10.1016/j.cell.2014.08.016

Guidi, C. J. *et al.* Disruption of Ini1 Leads to Peri-Implantation Lethality and Tumorigenesis in Mice. *Mol. Cell. Biol.* (2001). doi:10.1128/mcb.21.10.3598-3603.2001

Hansen, C. G., Moroishi, T. & Guan, K. L. YAP and TAZ: A nexus for Hippo signaling and beyond. *Trends in Cell Biology* (2015). doi:10.1016/j.tcb.2015.05.002

Hansen, C. G., Moroishi, T. & Guan, K.-L. YAP and TAZ: a nexus for Hippo signaling and beyond. *Trends Cell Biol.* **25**, 499–513 (2015).

Hara, R. & Sancar, A. The SWI/SNF Chromatin-Remodeling Factor Stimulates Repair by Human Excision Nuclease in the Mononucleosome Core Particle. *Mol. Cell. Biol.* (2002). doi:10.1128/mcb.22.19.6779-6787.2002

Harvey, K. F., Zhang, X. & Thomas, D. M. The Hippo pathway and human cancer. *Nature Reviews Cancer* (2013). doi:10.1038/nrc3458

He, X., Semenov, M., Tamai, K. & Zeng, X. LDL receptor-related proteins 5 and 6 in Wnt/β-catenin signaling: Arrows point the way. *Development* (2004). doi:10.1242/dev.01117

Helming, K. C., Wang, X. & Roberts, C. W. M. Vulnerabilities of mutant SWI/SNF complexes in cancer. *Cancer Cell* (2014). doi:10.1016/j.ccr.2014.07.018

Ho, L. *et al.* An embryonic stem cell chromatin remodeling complex, esBAF, is essential for embryonic stem cell self-renewal and pluripotency. *Proc. Natl. Acad. Sci. U. S. A.* (2009). doi:10.1073/pnas.0812889106

Hu, G. *et al.* Regulation of nucleosome landscape and transcription factor targeting at tissue-specific enhancers by BRG1. *Genome Res.* (2011). doi:10.1101/gr.121145.111

Huch, M. *et al.* In vitro expansion of single Lgr5 + liver stem cells induced by Wnt-driven regeneration. *Nature* (2013). doi:10.1038/nature11826

Huch, M. & Koo, B. K. Modeling mouse and human development using organoid cultures. *Development (Cambridge)* (2015). doi:10.1242/dev.118570

Jiao, Y. *et al.* Exome sequencing identifies frequent inactivating mutations in BAP1, ARID1A and PBRM1 in intrahepatic cholangiocarcinomas. *Nat. Genet.* (2013). doi:10.1038/ng.2813

Kadoch, C. & Crabtree, G. R. Mammalian SWI/SNF chromatin remodeling complexes and cancer: Mechanistic insights gained from human genomics. *Science Advances* (2015). doi:10.1126/sciadv.1500447

Kang, L., Wang, J., Zhang, Y., Kou, Z. & Gao, S. iPS Cells Can Support Full-Term Development of Tetraploid Blastocyst-Complemented Embryos. *Cell Stem Cell* (2009). doi:10.1016/j.stem.2009.07.001

Katano, T. *et al.* Establishment of a long-term three-dimensional primary culture of mouse glandular stomach epithelial cells within the stem cell niche. *Biochem. Biophys. Res. Commun.* (2013). doi:10.1016/j.bbrc.2013.02.051

Kidder, B. L., Palmer, S. & Knott, J. G. SWI/SNF-Brg1 Regulates Self-Renewal and Occupies Core Pluripotency-Related Genes in Embryonic Stem Cells. *Stem Cells* (2009). doi:10.1634/stemcells.2008-0710

Klochendler-Yeivin, A. *et al.* The murine SNF5/INI1 chromatin remodeling factor is essential for embryonic development and tumor suppression. *EMBO Rep.* (2000). doi:10.1093/embo-reports/kvd129

Koo, B. K. *et al.* Tumour suppressor RNF43 is a stem-cell E3 ligase that induces endocytosis of Wnt receptors. *Nature* (2012). doi:10.1038/nature11308

Lamar, J. M. *et al.* The Hippo pathway target, YAP, promotes metastasis through its TEAD-interaction domain. *Proc. Natl. Acad. Sci. U. S. A.* (2012). doi:10.1073/pnas.1212021109

Lau, A. N. *et al.* Tumor-propagating cells and Yap/Taz activity contribute to lung tumor progression and metastasis. *EMBO J.* (2014). doi:10.1002/embj.201386082

Lee, S. H. *et al.* Tumor Evolution and Drug Response in Patient-Derived Organoid Models of Bladder Cancer. *Cell* (2018). doi:10.1016/j.cell.2018.03.017

Li, X. *et al.* Oncogenic transformation of diverse gastrointestinal tissues in primary organoid culture. *Nat. Med.* (2014). doi:10.1038/nm.3585

Mahe, M. M. *et al.* Establishment of Gastrointestinal Epithelial Organoids. *Curr. Protoc. Mouse Biol.* (2013). doi:10.1002/9780470942390.mo130179

Martin-Belmonte, F. & Perez-Moreno, M. Epithelial cell polarity, stem cells and cancer. *Nature Reviews Cancer* (2012). doi:10.1038/nrc3169

Mou, H. *et al.* Dual SMAD Signaling Inhibition Enables Long-Term Expansion of Diverse Epithelial Basal Cells. *Cell Stem Cell* (2016). doi:10.1016/j.stem.2016.05.012

Moya, I. M. & Halder, G. The Hippo pathway in cellular reprogramming and regeneration of different organs. *Current Opinion in Cell Biology* (2016). doi:10.1016/j.ceb.2016.08.004

O'Rourke, K. P. *et al.* Transplantation of engineered organoids enables rapid generation of metastatic mouse models of colorectal cancer. *Nat. Biotechnol.* (2017). doi:10.1038/nbt.3837

Ootani, A. *et al.* Sustained in vitro intestinal epithelial culture within a Wnt-dependent stem cell niche. *Nat. Med.* (2009). doi:10.1038/nm.1951

Panciera, T. *et al.* Induction of Expandable Tissue-Specific Stem/Progenitor Cells through Transient Expression of YAP/TAZ. *Cell Stem Cell* (2016). doi:10.1016/j.stem.2016.08.009

Park, J. H. *et al.* Mammalian SWI/SNF complexes facilitate DNA double-strand break repair by promoting γ-H2AX induction. *EMBO J.* (2006). doi:10.1038/sj.emboj.7601291

Pei, T. *et al.* YAP is a critical oncogene in human cholangiocarcinoma. *Oncotarget* (2015). doi:10.18632/oncotarget.4043

Piccolo, S., Dupont, S. & Cordenonsi, M. The biology of YAP/TAZ: Hippo signaling and beyond. *Physiol. Rev.* (2014). doi:10.1152/physrev.00005.2014

Ramos, A. & Camargo, F. D. The Hippo signaling pathway and stem cell biology. *Trends in Cell Biology* (2012). doi:10.1016/j.tcb.2012.04.006

Reyes, J. C. *et al.* Altered control of cellular proliferation in the absence of mammalian brahma (SNF2α). *EMBO J.* (1998). doi:10.1093/emboj/17.23.6979

Roberts, C. W. M., Galusha, S. A., McMenamin, M. E., Fletcher, C. D. M. & Orkin, S. H. Haploinsufficiency of Snf5 (integrase interactor 1) predisposes to malignant rhabdoid tumors in mice. *Proc. Natl. Acad. Sci. U. S. A.* (2000). doi:10.1073/pnas.250492697

Roberts, C. W. M., Leroux, M. M., Fleming, M. D. & Orkin, S. H. Highly penetrant, rapid tumorigenesis through conditional inversion of the tumor suppressor gene Snf5. *Cancer Cell* (2002). doi:10.1016/S1535-6108(02)00185-X

Sachs, N. *et al.* A Living Biobank of Breast Cancer Organoids Captures Disease Heterogeneity. *Cell* (2018). doi:10.1016/j.cell.2017.11.010

Sato, T. & Clevers, H. Growing Self-Organizing Mini-Guts. *Science (80-.).* (2013).

Schuler, M., Dierich, A., Chambon, P. & Metzger, D. Efficient temporally controlled targeted somatic mutagenesis in hepatocytes of the mouse. *Genesis* (2004). doi:10.1002/gene.20039

Schwank, G. *et al.* Functional repair of CFTR by CRISPR/Cas9 in intestinal stem cell organoids of cystic fibrosis patients. *Cell Stem Cell* (2013). doi:10.1016/j.stem.2013.11.002

Singhal, N. *et al.* Chromatin-remodeling components of the baf complex facilitate reprogramming. *Cell* (2010). doi:10.1016/j.cell.2010.04.037

Smith, A. G. Embryo-Derived Stem Cells: Of Mice and Men. *Annu. Rev. Cell Dev. Biol.* (2001). doi:10.1146/annurev.cellbio.17.1.435

Stewart, S. A. *et al.* Lentivirus-delivered stable gene silencing by RNAi in primary cells. *RNA* (2003). doi:10.1261/rna.2192803

Stingl, J. *et al.* Purification and unique properties of mammary epithelial stem cells. *Nature* (2006). doi:10.1038/nature04496

Su, T. *et al.* Two-signal requirement for growth-promoting function of yap in hepatocytes. *Elife* (2015). doi:10.7554/eLife.02948

Takahashi, K. & Yamanaka, S. Induction of Pluripotent Stem Cells from Mouse Embryonic and Adult Fibroblast Cultures by Defined Factors. *Cell* (2006). doi:10.1016/j.cell.2006.07.024

Takahashi, T. Organoids for Drug Discovery and Personalized Medicine. *Annu. Rev. Pharmacol. Toxicol.* (2019). doi:10.1146/annurev-pharmtox-010818-021108

Tolstorukov, M. Y. *et al.* Swi/Snf chromatin remodeling/tumor suppressor complex establishes nucleosome occupancy at target promoters. *Proc. Natl. Acad. Sci. U. S. A.* (2013). doi:10.1073/pnas.1302209110

Van De Wetering, M. *et al.* Prospective derivation of a living organoid biobank of colorectal cancer patients. *Cell* (2015). doi:10.1016/j.cell.2015.03.053

Versteege, I. *et al.* Truncating mutations of hSNF5/INI1 in aggressive paediatric cancer. *Nature* (1998). doi:10.1038/28212

Visvader, J. E. & Lindeman, G. J. Cancer stem cells: Current status and evolving complexities. *Cell Stem Cell* (2012). doi:10.1016/j.stem.2012.05.007

Wang, D. *et al.* Identification of multipotent mammary stemcells by protein C receptor expression. *Nature* (2015). doi:10.1038/nature13851

Watanabe, K. *et al.* A ROCK inhibitor permits survival of dissociated human embryonic stem cells. *Nat. Biotechnol.* (2007). doi:10.1038/nbt1310

Watanabe, R. *et al.* SWI/SNF factors required for cellular resistance to dna damage include arid1a and arid1b and show interdependent protein stability. *Cancer Res.* (2014). doi:10.1158/0008-5472.CAN-13-3608

Wilson, B. G. & Roberts, C. W. M. SWI/SNF nucleosome remodellers and cancer. *Nature Reviews Cancer* (2011). doi:10.1038/nrc3068

Wu, J. I., Lessard, J. & Crabtree, G. R. Understanding the Words of Chromatin Regulation. *Cell* (2009). doi:10.1016/j.cell.2009.01.009

Yan, Z. *et al.* BAF250B-Associated SWI/SNF Chromatin-Remodeling Complex Is Required to Maintain Undifferentiated Mouse Embryonic Stem Cells. *Stem Cells* (2008). doi:10.1634/stemcells.2007-0846

Yimlamai, D. *et al.* Hippo pathway activity influences liver cell fate. *Cell* (2014). doi:10.1016/j.cell.2014.03.060

Young, D. W. *et al.* SWI/SNF chromatin remodeling complex is obligatory for BMP2-induced, Runx2-dependent skeletal gene expression that controls osteoblast differentiation. *J. Cell. Biochem.* (2005). doi:10.1002/jcb.20332

Yu, Y. *et al.* Olig2 targets chromatin remodelers to enhancers to initiate oligodendrocyte differentiation. *Cell* (2013). doi:10.1016/j.cell.2012.12.006

Yui, S. *et al.* YAP/TAZ-Dependent Reprogramming of Colonic Epithelium Links ECM Remodeling to Tissue Regeneration. *Cell Stem Cell* (2018). doi:10.1016/j.stem.2017.11.001

Zhang, N. *et al.* The Merlin/NF2 Tumor Suppressor Functions through the YAP Oncoprotein to Regulate Tissue Homeostasis in Mammals. *Dev. Cell* (2010). doi:10.1016/j.devcel.2010.06.015

Zhang, W. *et al.* Downstream of mutant KRAS, the transcription regulator YAP is essential for neoplastic progression to pancreatic ductal adenocarcinoma. *Sci. Signal.* (2014). doi:10.1126/scisignal.2005049

Zhao, B., Kim, J., Ye, X., Lai, Z. C. & Guan, K. L. Both TEAD-binding and WW domains are required for the growth stimulation and oncogenic transformation activity of yes-associated protein. *Cancer Res.* (2009). doi:10.1158/0008-5472.CAN-08-2997